Climate change drives rapid warming and increasing heatwaves of lakes

Wang, Xiwen; Shi, Kun; Zhang, Yunlin; Qin, Boqiang; Zhang, Yibo; Wang, Weijia; Woolway, R Iestyn; Piao, Shilong; Jeppesen, Erik

Science bulletin

DOI:
10.1016/j.scib.2023.06.028

Published: 30/07/2023

Climate change drives rapid warming and increasing heatwaves of lakes

Xiwen Wang [a, b], Kun Shi [a, c, d, *], Yunlin Zhang [a, c, d, *], Boqiang Qin [a], Yibo Zhang [a], Weijia Wang [a, c, d], R. Iestyn Woolway [e], Shilong Piao [f–h], Erik Jeppesen [i–l]

[a] Taihu Laboratory for Lake Ecosystem Research, State Key Laboratory of Lake Science and Environment, Nanjing Institute of Geography and Limnology, Chinese Academy of Sciences, Nanjing 210008, China

[b] Key Laboratory of Western China's Environmental Systems (Ministry of Education), College of Earth and Environmental Sciences, Lanzhou University, Lanzhou, 730000, China

[c] University of Chinese Academy of Sciences, Beijing 100049, China

[d] College of Nanjing, University of Chinese Academy of Sciences, Nanjing 2111, China

[e] School of Ocean Sciences, Bangor University, Menai Bridge, Anglesey, UK

[f] Sino-French Institute for Earth System Science, College of Urban and Environmental Sciences, Peking University, Beijing, China

[g] Key Laboratory of Alpine Ecology, Institute of Tibetan Plateau Research, Chinese Academy of Sciences, Beijing, China

[h] Center for Excellence in Tibetan Earth Science, Chinese Academy of Sciences, Beijing, China

[i] Department of Ecoscience, Aarhus University, Aarhus C, 8000, Denmark

[j] Sino-Danish Centre for Education and Research, Beijing, China

[k] Limnology Laboratory, Department of Biological Sciences and Centre for Ecosystem Research and Implementation (EKOSAM), Middle East Technical University, Ankara, 06800, Türkiye

[l] Institute of Marine Sciences, Middle East Technical University, Erdeneli-Mersin, 33731, Turkey

***Corresponding author**: Kun Shi and Yunlin Zhang, Nanjing Institute of Geography and Limnology, Chinese Academy of Sciences, 73 East Beijing Road, Nanjing 210008, P. R. China, Tel: + 86-25-86882008, Email: kshi@niglas.ac.cn, ylzhang@niglas.ac.cn

Abstract

Climate change could seriously threaten global lake ecosystems by warming lake surface water and increasing the occurrence of lake heatwaves. Yet, there are great uncertainties in quantifying lake temperature changes globally due to a lack of accurate large-scale model simulations. Here, we integrated satellite observations and a numerical model to improve lake temperature modeling and explore the multifaceted characteristics of trends in surface temperatures and lake heatwave occurrence in Chinese lakes from 1980 to 2100. Our model-data integration approach revealed that the lake surface waters have warmed at a rate of 0.11 °C $decade^{-1}$ during the period 1980–2021, being only half of the pure model-based estimate. Moreover, our analysis suggested that an asymmetric seasonal warming rate has led to a reduced temperature seasonality in eastern plain lakes but an amplified one in alpine lakes. The durations of lake heatwaves have also increased at a rate of 7.7 days $decade^{-1}$. Under the high-greenhouse-gas-emission scenario, lake surface temperature and lake heatwave duration were projected to increase by 2.2 °C and 197 days at the end of the 21st century, respectively. Such drastic changes would worsen the environmental conditions of lakes subjected to high and increasing anthropogenic pressures, posing great threats to aquatic biodiversity and human health.

Keywords: lake water temperature, numerical model, satellite observations, climate change

1. Introduction

Global lakes store 87% of Earth's liquid surface freshwater [1] and provide numerous critically important ecosystem services to human society [2]. However, lake ecosystems worldwide are already under severe threats from anthropogenic pressures and climate change. Lake surface water temperature (LSWT), an important physical indicator of the lake environment, is highly sensitive to climate change [3]. Evidence is mounting that lake surface warming – especially an increasing occurrence of lake heatwaves – has significantly affected the physical and chemical environment of aquatic systems [4, 5] and, ultimately, biodiversity and human health [6, 7]. But great uncertainties remain as to the quantification of lake temperature changes from regional [8-10] to global scales [11, 12]. The common approaches used to characterize lake temperature change include ground observations, satellite data, and numerical simulations, but they yield results that are not often comparable [12-14]. Ground observations of lake surface temperature are traditionally considered the most accurate but are scarcely and unevenly distributed both regionally and globally. For example, only summertime ground data observations of 151 lakes are included in the global lake temperature collaboration (GLTC), with nearly 80% of the data concentrated in Western Europe and North America [15]. Although satellite data could provide information on LSWT across large spatial scales [15] and, indeed, help to fill the void in global lake observations, a temporally consistent estimate of lake surface temperature using satellite sensors is only possible during the cloud-free period. Furthermore, satellite observations of lake surface temperature could be influenced by the thermal characteristics of adjacent lands, especially for small lakes, thus contaminating the lake surface temperature signal. In contrast to satellite products and ground measurements, numerical lake models can provide a spatially-explicit estimate of high temporal resolution lake surface temperature at a longer time scale [13, 16]. However, the accuracy of the modeled lake surface temperatures is often questioned due to the simplified representation of physical processes in model structures, the uncertainties of atmospheric forcings, and poor parameterization of lake-specific parameters. For instance, they are often replaced with a predefined value or empirical formula or calibrated based on the patterns revealed by the limited observations available [17, 18].

China has a total lake area of 81414.6 km^2. The lakes support nearly half of China's national centralized drinking water sources, and play critical roles in ecosystem services for human beings [19, 20]. The ongoing drastic climate change, together with rapid urbanization and economic growth, has greatly reshaped the thermal conditions of lakes over the past four decades. Furthermore, lakes in China have variable characteristics and geographical locations and have therefore been exposed to a wide variety of climate change factors [21], potentially generating spatially-varying impacts on changes in lake thermal conditions. However, existing global investigations have not explored Chinese lakes in detail [12]. How lake surface temperature and lake heatwaves change across China remain elusive, and little is known about how they will change under different climate change scenarios. Such knowledge is urgently needed, indeed, to improve our understanding of the processes and mechanisms underlying climate change impacts on Chinese lakes.

Here, we integrated, in a novel way, satellite observations with a numerical lake model to explore the multifaceted characteristics of surface warming and heatwaves using data from Chinese lakes during the period from 1980 to 2100 as an example. Specifically, we proposed a framework that auto-calibrates model parameters for each lake simulated by the Freshwater Lake model (FLake) [22] by assimilating satellite-derived LSWT from the European Space Agency Climate Change Initiative project (ESACCI; 2000–2020). The assimilation of satellite observations could overcome the large-scale parameterization limitation of FLake and provide an effective and accurate approach to estimating lake surface warming across large spatial and temporal scales. Our results showed widespread warming and increased heatwaves in Chinese lakes during the past four decades. Lake heatwaves were projected to become stronger and more prolonged by the end of the twenty-first century.

2. Materials and methods

2.1 Study sites

We selected 168 lakes with a surface area ≥ 50 km^2, as defined in the HydroLAKES database [1], and with more than 100 valid cloud-free satellite retrievals during 2000–2020 (see Materials and methods). The lakes ranged between 0 and 5387 m in altitude, between 24.5 and 49.0 °N in latitude, between 50.0 and 4266.6 km^2 in surface area, and between 1.1 and 120 m in average depth (Figure S1; Table S2). These lakes covered all five lake regions in China [19], i.e., the Northeast Plain and Mountain Lake (NPML), Inner Mongolia-Xinjiang Lake (IMXL), Tibetan Plateau Lake (TPL), Eastern Plain Lake (EPL), and Yunnan-Guizhou Plateau Lake (YGPL).

2.2 FLake model

The FLake model is a one-dimensional bulk model based on the concept of self-similarity, where the vertical profiles of lake ice, the mixed layer, the thermocline, and the thermally active upper layer of sediments are described by their own shape functions [23], which contributes to its low computational cost. FLake has been implemented into large-scale lake simulations [16, 24, 25] and global weather prediction models [23, 26]. It has been widely tested on lakes in China [27-30]. The meteorological variables required to drive FLake include 2 m air temperature, 10 m wind speed, 2 m specific humidity, surface pressure, surface downward shortwave radiation, and surface downward longwave radiation. Lake-specific characteristics also need to be described for each lake, including average depth, fetch, light extinction coefficient, and latitude. The snow module of FLake, which is currently under development, was turned off in our study. Regarding the bottom sediment module, we adopted the suggestions from the model's official site – that the heat exchange between lake water and sediments is only important for shallow lakes and that the heat fluxes at the water-sediment interface can be neglected when the lake depth is larger than 5 m. The lake fetch (km) was calculated from the lake surface area (km^2) as

$fetch = 39.9 + 0.00781 \times surface\ area$ [17].

The wind speed over land at latitudes > 35°N was scaled by $U_{water} = 1.62 + 1.17U_{land}$ [17], where U_{water} is the wind speed over water (m s^{-1}) and U_{land} is the wind speed over land (m s^{-1}). We ran the FLake model from January 1st 1950 and repeated the first 365 days as the model spin-up. The model simulation results since 1980 were analyzed as the drastic economic growth of China and the rapid warming in Northern Hemisphere lakes started in this year [31].

2.3 Datasets and the experimental design

Climate forcing from ERA5-Land [32] was used to run FLake for the historical period. ERA5-Land was available at a grid resolution of 0.1° × 0.1° and at an hourly time interval.

Five downscaled global climate model projections of the NASA Earth Exchange Global Daily Downscaled Projections (NEX-GDDP-CMIP6) [33], i.e., FGOALS-g3, GFDL-ESM4, MPI-ESM1-2-HR, MRI-ESM2-0, and UKESM1-0-LL, were selected for the future projections relative to four shared socioeconomic pathways (SSPs): SSP1-2.6, SSP2-4.5, SSP3-7.0, and SSP5-8.5, representing a radiative forcing of 2.6, 4.5, 3.7, and 8.5 W m^{-2} by 2100, respectively. These data were available at daily time steps and a spatial resolution of 0.25° × 0.25°. The historical (1950–2014) and scenario (2015–2100) data from NEX-GDDP-CMIP6 were concatenated to run FLake. For both ERA5-Land and NEX-GDDP-CMIP6, we extracted the time series of the closest grid points from the center of the lakes as model inputs.

The satellite-derived LSWT from the ESACCI project [34] was used as a reference for assessing FLake model performances. ESACCI provided daily LSWT data on more than 2000 inland water bodies worldwide at a resolution of 1 km during 1992–2020. We filtered the data with its quality flag and selected the best level only and interpolated ESACCI to the centroids of each lake to acquire a “mean” state of the lake center.

We collected ground observations of LSWT from nine lakes (Table S1) to verify the credibility of our model results, including both plain/alpine warm lakes and boreal/alpine cold lakes with diverse thermal regimes. These data were documented at hourly to monthly intervals, generally from 1993 to 2020.

We used the human footprint index (HFI) to analyze the impact of anthropogenic stressors on lake temperature, including the effects of building, cropland, pasture, population density, night light, railways, roads, seaways, etc. The HFI dataset used in this study [35] represents the human activity intensity in 2019 and has a spatial resolution of 0.00989°. HFI values range from 0 to 1, indicating low to high anthropogenic influence.

2.4 The workflow of CSFLake

The novel approach introduced here is referred to as CSFLake (Coupling remote Sensing observations and FLake). We first calibrated and validated the model parameters in FLake over the periods 2001–2010 and 2011–2020 using the workflow of CSFLake as follows. Then we ran our CSFLake with the best parameters to acquire the historical (1950–2021) and future (2015–2100) LSWT.

We selected three important in-lake model parameters to improve model performances: light extinction coefficient, lake ice albedo, and depth factor. The light extinction coefficient determines the amount of shortwave radiation penetrating the deep layers of the lake and affects the surface water temperature, especially in summer [17]. In the FLake model, it is 3 m^{-1} by default. We set the range of light extinction coefficients to 0.1–0.3 m^{-1} for the lakes on the Tibetan Plateau, which have the most transparent water [36], and to 0.1–3 m^{-1} for the remaining lakes. The ice albedo is the percentage of incoming solar radiation that is reflected into the atmosphere and thus controls the rate of ice melt and the thaw date [17]. In the default FLake model, it is computed from the albedo of white and blue ice and varies with surface temperature. To maximize the efficiency of the calibration procedure, we set the lake ice albedo as a unique constant and altered its value to 0.1–0.85, which is within the range of observations [37]. The depth factor was used to set an "effective depth" for each lake [17, 38], which is widely used in FLake modeling studies to compensate for the uncertainty in lake depth estimates. Deep lakes have larger thermal inertia, a lower summer surface temperature, and a later freeze date [17]. We set the range of depth factors to 0.25–4 [38].

Latin Hypercube Sampling (LHS) is a stratified sampling method used for Monte Carlo simulation [39]. Compared with pure random sampling, the pseudo-random procedure of LHS generates more evenly distributed samples and achieves satisfactory accuracy with a smaller sample size, which results in less computational cost. The LHS method has been applied as one of the auto-calibration algorithms in a lake modeling package [40]. We first sampled 300 values within the prescribed valid range and preserved the parameter sets that get optimum results, i.e., the highest Pearson correlation coefficient with ESACCI.

Some lakes still show poor fitness because of the delayed ice-off on the Tibetan Plateau; this is possibly due to the absence of snow whose insulation effect could prevent ice thickening [41]. We further narrowed the valid range of the ice albedo to 0.1–0.3 to allow more shortwave radiation to be absorbed by the ice cover and accelerate the melting process.

Although the obtained parameters may not be realistic for some lakes, they can serve as a proxy for processes that have not been included in the model [30], for example, salinity for non-freshwater lakes, horizontal advection, intrusion of groundwater or glacial melt water, which constitute important inflows in lakes on the Tibetan Plateau.

2.5 Lake heatwaves

A lake heatwave is defined as when the daily LSWT exceeds the 90% threshold of the seasonally varying climatology period for at least five consecutive days [16, 42]. We selected 1980–2009 as the climatology period while calculating the heatwave for the historical and future simulations. We followed the same computation method as in a previous study [16] but excluded heatwave events occurring when the threshold value is less than the climatology value. This could happen in some lakes that have regular ice cover but do not freeze for a few years. The annual mean lake heatwave maximum intensity (maximum temperature anomaly relative to the climatological mean in an event) and total annual days (time between the start and end dates of an event) were computed in each year as metrics for heatwaves. We categorized lake heatwaves into four groups depending on their duration: 5–15 days for short events, 15–25 days for medium events, 25–35 days for long events, and above 35 days for prolonged events. The lake heatwave events were detected from the daily simulated LSWT using the Python package "marineHeatWaves" (www.github.com/ecjoliver/marineHeatWaves).

2.6 Contribution analysis

We performed six simulations, denoted as S1–6, for the period 1979–2021 using climate fields from ERA5-Land. The control simulation (CTL) was a subset of the historical simulation. In the S1–6 simulations, air temperature (AT), wind speed (U), surface pressure

(P), surface shortwave (SW) and longwave radiation (LW), and specific humidity (Q) were kept unchanged as 1979, while the remaining variables varied as in the CTL. The contributions of each meteorological variable are represented by the percent relative change from the LSWT trend in CTL to those in S1–6 simulations.

To attribute the drivers of lake heatwaves, we used the fraction of attributable risk [43] (FAR) to quantify the influences of each meteorological variable on the likelihood of occurrence of long lake heatwaves. FAR quantifies the impacts of cause A on an event by comparing the likelihood of such events in the real world (the world with the cause A) and the counterfactual world (the world in which cause A is absent), and it has been used previously to quantify the impacts of anthropogenic climate change on the intensity of lake heatwaves [44]. We calculated FAR as FAR = $1 - P_0 / P_1$, where P_1 is the probability that a long heatwave event occurred in the actual world (i.e., CTL), and P_0 is the probability that a long heatwave event occurred in the counterfactual worlds (S1–6). Any negative resulting value will be assigned to zero. The value of FAR represents the likelihood that a potential factor will be the necessary causation of a long heatwave event. For example, if the FAR calculated from S1 for Lake B is 90%, it means that 90% of the probability of a long event in B is due to the trend of air temperature or that there is a 90% chance that the air temperature trend is necessary for a long event to occur in B.

2.7 Time series analysis

For the raw simulation results for each lake, we set the minimum water temperature as 1 °C [17] to filter the ice coverage periods. To account for the mismatch between the simulated and satellite-observed ice period, frozen values were included but replaced with 1 °C while calculating model performance metrics (i.e., correlation coefficient and root mean square error [RMSE]) during the calibration and validation of CSFLake. However, during the trend analysis, we only focused on simulated water temperatures above 1 °C and excluded frozen values. The long-term trends and their confidence levels were calculated using the Theil-Sen estimator.

3. Results and discussion

3.1 Spatial distribution of LSWT using a blended analysis of a numerical model and satellite observations

Our satellite-derived constraint on the original FLake simulations accurately reproduced the satellite-based LSWT across both spatial and temporal scales (Figure 1). Overall, the model performances declined slightly but remained acceptable during the validation phase compared to the calibration phase (Figure S2). For both 2011–2020 and 2001–2010, the correlation coefficient between simulation results and satellite observations was 0.97 ± 0.02 (the uncertainty means the standard deviation across lakes). The RMSE for 2011–2020 was 1.31 ± 0.32 °C and 1.35 ± 0.35 °C for 2001–2010. Over the entire satellite data-taking period, the correlation coefficient increased from 0.79 to 0.97 and RMSE decreased from 4.46 to 1.39 °C, indicating substantial improvements. Compared to ground observations (Table S1), CSFLake also produced satisfactory results (Figure S3; Figure S4). The comparison with daily observations showed correlation coefficients larger than 0.96 and RMSE ranging between 0.94 and 1.50 °C. We also achieved satisfactory accuracy at hourly and sub-hourly intervals with RMSEs of 1.19 °C and 1.67 °C, although the model parameters were determined by daily satellite observations. The original FLake model well captured the LSWT in shallow and warm lakes on the Eastern Plain and Yunnan-Guizhou Plateau, whereas considerable bias occurred for ice-covered lakes on the Tibetan Plateau (RMSE = 4.80 °C). Four Tibetan lakes were even simulated to remain frozen throughout the year. These model biases are in part attributed to the absence of saline effects on lake temperature and the effects of snow insulation on preventing ice thickening in FLake [45]. CSFLake overcame the deficiencies of the FLake model due to unknown lake-specific characteristics (e.g., water clarity and ice albedo) or missing processes (e.g., salinity and snow; see Materials and methods). Given the difficulty of monitoring lake interior information at large scales and the enormous accessible satellite data, CSFLake undoubtedly has advantages over pure model-based simulation. The flexibility and good performance demonstrated across diverse Chinese lakes, further support the future global application of CSFLake.

The annual mean climatology of LSWT (1980–2021) revealed an average LSWT of 11.2 °C across all the studied lakes but with a substantial spatial variation (Figure S5). Among the five lake zones considered, EPL has the highest annual mean LSWT (17.8°C), followed by YGPL (17.7°C), NPML (16.7°C), IMXL (12.1°C), and TPL (8.8°C). EPL and YGPL were the warmest due to their low latitudes, but the annual range of LSWT was much smaller in YGPL than in EPL as the summer heating is mitigated by its highlands. Unsurprisingly, TPL was the coldest of the five lake zones.

3.2 Changes in LSWT and heatwave characteristics from 1980 to 2021

Our results suggested that LSWT in the studied Chinese lakes has experienced rapid warming over the past four decades. During 1980–2021, the annual mean LSWT across Chinese lakes significantly increased at a rate of 0.11 °C decade^{-1} ($p < 0.01$) (Figure 2a), while the original FLake overestimated the warming trend by about 100%, especially for Tibetan lakes (Figure S6). This implies that the model parameters should be carefully calibrated to avoid systematic errors in the estimation of long-term trends.

The spatial distribution of LSWT trends showed clear altitudinal and latitudinal dependences, with plain and subtropical lakes warming faster than alpine and boreal lakes, respectively (Figure S7a; Figure 2d). If the warming trend was normalized by its climatology, boreal, and alpine lakes, particularly TPL, would have the most significant trend (Figure S8). Among the five lake zones, the average warming trend was higher in the warmer (i.e., lakes with higher climatological annual mean LSWT) and shallower lakes (Figure S9a&b). For example, EPL had a larger warming rate (0.22 °C decade^{-1}) than the other lake zones (0.08 to 0.12 °C decade^{-1}) (Figure 2d; Figure S9e). Moreover, we found that the warming trend in five lake zones increased with the intensity of human activity, as indicated by HFI in 2019 (Figure S9f). This suggests that the emission of greenhouse gases and rapid urbanization, which have been identified as the primary causes of the extreme summer air temperatures in eastern China [46], accelerated lake surface warming.

The lake warming rates across China were considerably smaller than the global average [12] (0.34 °C decade^{-1}), which only includes 15 Chinese lakes. In contrast to temperate lakes with seasonal ice cover [3], alpine lakes on the Tibetan Plateau experienced much less warming. This demonstrates how the performance of lake temperature simulation results, particularly for Tibetan lakes, can significantly bias estimates of lake warming. In addition, a previous LSWT analysis using satellite products across Chinese lakes indicated a much higher warming rate of 0.26 °C decade^{-1} ($p < 0.01$) in 2001–2016 than our model-data blended analysis (0.03 °C decade^{-1}, $p > 0.05$) during the same period, i.e. 2001–2016 [47]. This discrepancy is possibly due to the inclusion of ice temperature in the previous satellite-based analysis and the large temporal interval of the available data (≥ 8 days). Our insignificant warming trend is consistent with the change in global air temperature during the "warming hiatus" period [48].

At seasonal timescales, the warming trend of Chinese lakes was uneven (Figure S10). The annual maximum LSWT had a mean rate of 0.14 °C decade^{-1} from 1980 to 2021, which is faster than the annual mean LSWT (Figure S11a). The annual maximum LSWT trends showed a clear latitudinal gradient, with lakes at higher latitudes exhibiting stronger trends.

The lakes generally displayed the highest warming rate in spring (March–May) for EPL and IMXL lakes. The warming rate in summer (June–August) and autumn (September–November) was most notable for NPML and TPL lakes with seasonal ice cover. By contrast, the warming rates of YGPL were roughly similar across different months, peaking in October (Figure S12b). The spring warming rate in EPL (0.45 °C decade^{-1}) was more than twice as high as the annual warming rate, with a maximum in March reaching 0.67 °C decade^{-1} (Figure S12b). This result is consistent with previous findings from four lakes in the Yangtze River basin, showing a warming rate of 0.26–0.28°C decade^{-1} (1979–2017) and that the warming rate in the spring was twice to four times higher than in other seasons [27]. Moreover, the ratio of spring to summer warming rates increased for low-altitude lakes and decreased for high-altitude lakes (Figure S13), suggesting that seasonality was reduced in plain lakes but amplified in alpine lakes due to asymmetric warming.

From 1980 to 2021, the climatological annual mean lake heatwave maximum intensity and total annual days across Chinese lakes had an average value of 1.6 °C and 21 days, respectively (Figure S14b). In terms of the spatial pattern, the average maximum intensity of lake heatwaves decreased with increasing altitude, with the highest intensity in eastern China (EPL and NPML; 3.5 and 3.7 °C) and the lowest at YGPL and TPL (1.0 and 1.1 °C). This result is possibly related to the lower variability of LSWT in alpine lakes (Figure S5b), which is consistent with previous findings that lakes with higher interannual variability experience stronger lake heatwaves [16]. The total annual days of lake heatwaves were larger for lakes located at lower latitudes, with YGPL experiencing the longest lake heatwaves. Moreover, TPL and YGPL endured the most prolonged lake heatwaves during the warm seasons (May–September; Figure S15d).

The maximum intensity of lake heatwaves showed a weak but significant increasing trend across Chinese lakes with a mean rate of 0.27 °C decade^{-1}, and the total annual days of lake heatwaves increased rapidly with an average rate of 7.7 days decade^{-1} (Figure 3a&b). A greater number of lakes had a significantly increasing trend in heatwave total annual days (154 of 168 lakes) than in heatwave maximum intensity (115 of 168 lakes). The heatwave maximum intensity increased most at EPL (0.30 °C $decade^{-1}$) and TPL (0.15 °C $decade^{-1}$), whereas the increasing rates of heatwave total annual days were greatest for the alpine lakes of YGPL (11.0 days $decade^{-1}$) and TPL (5.9 days $decade^{-1}$) (Figure 3c&d; Figure S7c&d).

We also found a strong negative correlation between lake depth and the maximum intensity of lake heatwaves (Figure S9c), suggesting that lake heatwaves were milder in deep lakes compared to shallow ones. Deep lakes generally had a longer duration of lake heatwaves (Figure S9d) because their greater thermal inertia increases their resistance to short-term climatic variations but also prevents them from quickly recovering from an extreme state. Furthermore, the lake heatwave maximum intensity was more strongly correlated with lake depth than the lake heatwave total annual days (−0.51 versus 0.27). Hence, morphological characteristics affect lake heatwave intensity more than duration.

3.3 Drivers of lake warming

Air temperature, specific humidity, and longwave radiation all increased across China from 1980 to 2021, but there were marked spatial differences in temporal variations of wind speed, shortwave radiation, and surface pressure (Figure S17). Our attribution analysis showed that longwave radiation (47.7%), specific humidity (39.4%), and air temperature (24.3%) were the major factors contributing to lake warming, although the magnitude of their respective contributions varied by season and lake zone (Figure 4a-e). We also calculated FAR to detect the necessary causation for a heatwave event to last more than 25 days, which we refer to as a "long event" (see Materials and methods). It appears that the FAR for these three variables (i.e., longwave radiation, specific humidity, and air temperature) was 1 for 50 lakes, which were mainly distributed in Eastern China and the Tibetan Plateau (Figure 4f; Figure S16), suggesting that these variables had a 100% chance of inducing a long heatwave event in these lakes. Shortwave radiation, surface pressure, and wind speed were also required for long heatwaves, with 71.3%, 73.9%, and 69.8% probability for 48, 36, and 34 lakes, respectively. It should be noted that our sensitivity experiments can only detect the isolated effects of meteorological variables on lake temperature. As a result, there are still lakes that failed to compute FAR, indicating that non-linear interactions between multiple meteorological factors may play an important role.

Increasing air temperature (Figure S17f) contributed most to the warming of the annual LSWT for EPL (41.8%), YGPL (58.3%), and IMXL (50.7%), whereas longwave radiation was the most important factor for TPL (79.5%). The increased shortwave radiation contributed to the lake surface warming in EPL, NPML, and YGPL, whereas the decreased shortwave radiation in TPL prevented lake surface warming (Figure S17d). The slow warming rate for Tibetan lakes can be explained by the dimming of solar radiation on the Tibetan Plateau, which is further related to the promoted deep convection by surface warming and moistening [49]. Tibetan Plateau lakes are typically warmer than the overlying atmosphere because of the strong solar radiation in the high-altitude region [50], and the influence of increasing air temperature may thus be counteracted by solar dimming [28]. However, this was not found in the pure modeling framework [51, 52], highlighting that great uncertainties exist in both the lake model itself and the LSWT data used for model calibration.

In spring, the combined effects of increasing air temperature, shortwave radiation, specific humidity, and longwave radiation led to a remarkable warming trend of LSWT in EPL (Figure 4c; Figure S10a). Moreover, the implementation of air pollution control policies since 2013 has greatly reduced aerosols, leading to an accelerated brightening in southeastern China [53]. This phenomenon could enhance the warming of lakes in eastern China (EPL and NPML) because of their relatively low water clarity [36]. The intense spring warming in EPL may impede the treatment of eutrophication by providing suitable thermal environments for harmful algae. The start dates of blooms in Lake Taihu have advanced by 30 days from 2003 to 2017 [54] and this could worsen in the future without interventions.

3.4 Future projections of LSWT and lake heatwaves

Annual mean LSWT, annual maximum LSWT, and the annual mean maximum intensity and total annual days of lake heatwaves are projected to increase substantially during the twenty-first century, with the magnitude of these changes increasing with the severity of climate change scenarios (Figure 5). Under the most stringent scenario (SSP1-2.6), relative to the period 1980–2009, the annual mean LSWT, annual maximum LSWT, heatwave annual mean maximum intensity, and heatwave total annual days (averaged during 2071–2100) will increase by 1.0 [0.7, 1.7] °C, 1.4 [0.9, 2.5] °C, 1.7 [1.2, 3.1] °C, and 119 [88, 180] days by the end of the century, respectively. The values within square brackets represent the minimum and maximum for the five climate model ensembles. Under the worst-case scenario (SSP5-8.5), the annual mean LSWT, annual maximum LSWT, heatwave annual mean maximum intensity, and heatwave total annual days will increase by 2.2 [1.8, 3.3] °C, 3.6 [2.8, 5.6] °C, 4.8 [3.9, 7.3] °C, and 197 [189, 218] days, respectively. In different lake zones, the strongest future warming of LSWT occurred at EPL, as also found for the historical period. By contrast, TPL had the greatest increase in the intensity of lake heatwaves, while EPL and YGPL had the greatest increase in the duration of lake heatwaves. Generally, lakes at lower latitudes will experience longer heatwaves.

Warmer surface water could have cascading effects on the physical and chemical environments of the aquatic systems (Figure 6). Lake thermal stratification will be strengthened because of the increasing temperature/density gradient between surface and bottom water [3]. Along with the warming lake surface in spring, thermal stratification will start earlier, thereby inhibiting the exchange of oxygen and nutrients between the lake surface and bottom [55] and increasing the summer surface temperature [7].

The lake surface warming will also result in reduced gas solubility, which is the primary factor of deoxygenation at the lake surface, although, in some productive lakes, this phenomenon could be diminished by the strengthened photosynthesis due to increasing phytoplankton biomass [56]. In the deep layer of lakes, the accelerated rates of respiration with warmer temperatures [5] will lead to higher oxygen consumption, but oxygen replenishment will be reduced by the stably stratified water column, and anoxic conditions will follow [56]. For example, within deep Lake Qiandao, the strong lake stratification in 2016 drastically reduced the dissolved oxygen in the thermocline and deep layers [57].

High water temperatures and low oxygen concentrations will squeeze the oxythermal habitat of fish [58, 59]. Rising annual maximum LSWT may even exceed the critical temperature allowing the normal physiological functions for species [60]. The dispersed distribution of lakes can dampen the movement of lacustrine species to suitable water, and the physical environment is projected to change more rapidly than the migration speeds of aquatic species [61], which might cause more ecological disasters.

At the water-sediment interface, anoxia will facilitate nutrient release from redox-sensitive compounds [62], especially phosphorus, which is a major limiting factor for algae growth in freshwater. If the bottom water temperature also increases, the mineralization of organic matter will be accelerated, which will lead to higher emissions of carbon dioxide and methane [63, 64], reinforcing climate warming due to greenhouse gases. This process will speed up the recycling of nutrients and favor phytoplankton growth, suggesting positive feedback between climate change and eutrophication [65].

Together with the heavy external nutrient loading from domestic, agricultural, and industrial waste, the growth of phytoplankton is promoted by hot water under nutrient-rich conditions [66]. Besides that, stronger stratification will permit phytoplankton to circulate in the euphotic zone [67]. Increasing algae blooms have been reported worldwide, especially in regions that depend highly on fertilizers [68]. In China, the occurrence of algae blooms in the 2010s has increased nearly nine times relative to the 1980s–1990s [68], and many blooms have been reported recently in natural lakes and reservoirs (Figure S18).

Furthermore, the warmer surface water and stronger stratification will favor the dominance of cyanobacteria in lakes given its higher optimal growth temperature and ability to adjust buoyancy [66], leading to a higher frequency of harmful algae blooms [64]. The toxic substances produced by cyanobacteria will threaten the security of drinking water and human health [6, 69]. For example, the unusually warm spring in Lake Taihu in 2007 triggered a cyanobacteria bloom that eventually contaminated the water supply for the two million inhabitants around the lake [6]. Blooms create turbid lake water and exhaust dissolved oxygen due to the decomposition process after they die, resulting also in massive die-offs of fishes [59]. Moreover, the photosynthesis-induced increases in pH during the blooms [62] and the subsequent low-oxygen conditions will stimulate the release of nutrients, creating positive feedback and deteriorating water quality.

4. Conclusion

Our study proposed a novel model–satellite data blended approach to investigate the changes in water temperature in 168 Chinese lakes from 1980 to 2100. During 1980–2021, the annual mean and annual maximum water temperature in China increased at an average rate of 0.11 °C decade^{-1} and 0.14 °C decade^{-1}, respectively. Among the five Chinese lake zones, the warming rate was highest in EPL and lowest in TPL. The water temperature in shallow, warm, and anthropogenic-affected lakes changed more rapidly than in other lakes. In general, longwave radiation, specific humidity, and air temperature contributed most to the increase of lake water temperature and the prolongation of lake heatwaves. Our projections showed that warming in Chinese lakes will continue into the twenty-first century, along with more intensive and prolonged lake heatwaves. Our results give opportunities for researchers and managers to enhance their understanding of the changing physical environment and formulate management or policies to alleviate the consequences of climate change in lakes.

Conflict of interest: The authors declare that they have no conflict of interest.

Acknowledgments

This study was supported by the National Natural Science Foundation of China (U22A20561 and 41922005), the Tibetan Plateau Scientific Expedition and Research Program, (2019QZKK0202), the National Key Research and Development Program of China (2022YFC3204100), and the NIGLAS foundation (E1SL002). EJ was supported by the Tübitak program BIDEB2232 (project 118C250). RIW was supported by a UKRI Natural Environment Research Council (NERC) Independent Research Fellowship [grant number NE/T011246/1]. We thank Anne Mette Poulsen for the valuable editions.

Author contributions

Xiwen Wang: Investigation, Conceptualization, Data curation, Methodology, Writing - original draft. **Kun Shi:** Supervision, Conceptualization, Methodology, and Editing. **Yunlin Zhang:** Data curation and Validation. **Yibo Zhang:** Methodology, Software, and Validation. **Boqiang Qin:** Conceptualization, Validation, and Editing. **Weijia Wang:** Data curation, Methodology, and Validation. **R. Iestyn Woolway:** Supervision and Editing. **Shilong Piao:** Supervision and Editing. **Jeppesen Erik:** Supervision and Editing. All authors reviewed the results and approved the final version of the manuscript.

References

[1] Messager ML, Lehner B, Grill G, et al. Estimating the volume and age of water stored in global lakes using a geo-statistical approach. Nat Commun 2016; 7: 13603.

[2] Costanza R, d'Arge R, de Groot R, et al. The value of the world's ecosystem services and

natural capital. Nature 1997; 387: 253-260.

[3] Woolway RI, Kraemer BM, Lenters JD, et al. Global lake responses to climate change. Nat Rev Earth Environ 2020; 1: 388-403.

[4] Anderson EJ, Stow CA, Gronewold AD, et al. Seasonal overturn and stratification changes drive deep-water warming in one of Earth's largest lakes. Nat Commun 2021; 12: 1688.

[5] Yvon-Durocher G, Jones JI, Trimmer M, et al. Warming alters the metabolic balance of ecosystems. Philos Trans R Soc Lond B: Biol Sci 2010; 365: 2117-2126.

[6] Qin B, Zhu G, Gao G, et al. A drinking water crisis in Lake Taihu, China: Linkage to climatic variability and lake management. Environ Manage 2010; 45: 105-112.

[7] Woolway RI, Sharma S, Smol JP. Lakes in hot water: The impacts of a changing climate on aquatic ecosystems. BioScience 2022; 72: 1050-1061.

[8] Schneider P, Hook SJ, Radocinski RG, et al. Satellite observations indicate rapid warming trend for lakes in California and Nevada. Geophys Res Lett 2009; 36: L22402.

[9] Torbick N, Ziniti B, Wu S, et al. Spatiotemporal lake skin summer temperature trends in the Northeast United States. Earth Interact 2016; 20: 1-21.

[10] Woolway RI, Dokulil MT, Marszelewski W, et al. Warming of Central European lakes and their response to the 1980s climate regime shift. Clim Change 2017; 142: 505-520.

[11] Schneider P, Hook SJ. Space observations of inland water bodies show rapid surface warming since 1985. Geophys Res Lett 2010; 37: L22405.

[12] O'Reilly CM, Sharma S, Gray DK, et al. Rapid and highly variable warming of lake

surface waters around the globe. Geophys Res Lett 2015; 42: 10773-10781.

[13] Grant L, Vanderkelen I, Gudmundsson L, et al. Attribution of global lake systems change to anthropogenic forcing. Nat Geosci 2021; 14: 849-854.

[14] Wan W, Zhao L, Xie H, et al. Lake surface water temperature change over the Tibetan Plateau from 2001 to 2015: A sensitive indicator of the warming climate. Geophys Res Lett 2018; 45: 11177-11186.

[15] Sharma S, Gray DK, Read JS, et al. A global database of lake surface temperatures collected by in situ and satellite methods from 1985-2009. Sci Data 2015; 2: 1-19.

[16] Woolway RI, Jennings E, Shatwell T, et al. Lake heatwaves under climate change. Nature 2021; 589: 402-407.

[17] Layden A, MacCallum SN, Merchant CJ. Determining lake surface water temperatures worldwide using a tuned one-dimensional lake model. Geosci Model Dev 2016; 9: 2167-2189.

[18] Woolway RI, Merchant CJ. Worldwide alteration of lake mixing regimes in response to climate change. Nat Geosci 2019; 12: 271-276.

[19] Ma R, Yang G, Duan H, et al. China’s lakes at present: Number, area and spatial distribution. Sci China: Earth Sci 2010; 54: 283-289.

[20] Zhang Y, Deng J, Qin B, et al. Importance and vulnerability of lakes and reservoirs supporting drinking water in China. Fundam Res 2022; 1-9.

[21] Tao S, Fang J, Ma S, et al. Changes in China's lakes: Climate and human impacts. Natl Sci Rev 2020; 7: 132-140.

[22] Mironov DV. Parameterization of lakes in numerical weather prediction: Description of a lake model. Deutscher Wetterdienst, Offenbach; 2008.

[23] Mironov D, Heise E, Kourzeneva E, et al. Implementation of the lake parameterisation scheme FLake into the numerical weather prediction model COSMO. Boreal Environ Res 2010; 15: 218–230.

[24] Maberly SC, O'Donnell RA, Woolway RI, et al. Global lake thermal regions shift under climate change. Nat Commun 2020; 11: 1232.

[25] Woolway RI, Sharma S, Weyhenmeyer GA, et al. Phenological shifts in lake stratification under climate change. Nat Commun 2021; 12: 2318.

[26] Balsamo G, Salgado R, Dutra E, et al. On the contribution of lakes in predicting near-surface temperature in a global weather forecasting model. Tellus A: Dyn Meteorol 2012; 64: 15829.

[27] Li X, Peng S, Deng X, et al. Attribution of lake warming in four shallow lakes in the middle and lower Yangtze River basin. Environ Sci Technol 2019; 53: 12548-12555.

[28] Kirillin G, Wen L, Shatwell T. Seasonal thermal regime and climatic trends in lakes of the Tibetan highlands. Hydrol Earth Syst Sc 2017; 21: 1895-1909.

[29] Su D, Hu X, Wen L, et al. Numerical study on the response of the largest lake in China to climate change. Hydrol Earth Syst Sc 2019; 23: 2093-2109.

[30] Huang A, Lazhu, Wang J, et al. Evaluating and improving the performance of three 1-D Lake models in a large deep lake of the central Tibetan Plateau. J Geophys Res-atmos 2019; 124: 3143-3167.

[31] Piccolroaz S, Woolway RI, Merchant CJ. Global reconstruction of twentieth century lake surface water temperature reveals different warming trends depending on the climatic zone. Clim Change 2020; 160: 427-442.

[32] Muñoz-Sabater J, Dutra E, Agustí-Panareda A, et al. ERA5-Land: A state-of-the-art global reanalysis dataset for land applications. Earth Syst Sci Data 2021; 13: 4349-4383.

[33] Thrasher B, Wang W, Michaelis A, et al. NASA global daily downscaled projections, CMIP6. Sci Data 2022; 9: 262.

[34] Carrea L, Cretaux JF, Liu X, et al. Satellite-derived multivariate world-wide lake physical variable timeseries for climate studies. Sci Data 2023; 10: 30.

[35] Keys PW, Barnes EA, Carter NH. A machine-learning approach to human footprint index estimation with applications to sustainable development. Environ Res Lett 2021; 16: 044061.

[36] Zhang Y, Zhang Y, Shi K, et al. Remote sensing estimation of water clarity for various lakes in China. Water Res 2021; 192: 116844.

[37] Robinson AL, Ariano SS, Brown LC. The influence of snow and ice albedo towards improved lake ice simulations. Hydrology 2021; 8: 11.

[38] Huang L, Wang X, Sang Y, et al. Optimizing lake surface water temperature simulations over large lakes in China with FLake model. Earth Space Sci 2021; 8: e2021EA001737.

[39] McKay MD, Beckman RJ, Conover WJ. A comparison of three methods for selecting values of input variables in the analysis of output from a computer code. Technometrics 2000; 42: 55-61.

[40] Moore TN, Mesman JP, Ladwig R, et al. LakeEnsemblR: An R package that facilitates ensemble modelling of lakes. Environ Modell Softw 2021; 143: 105101.

[41] Sharma S, Meyer MF, Culpepper J, et al. Integrating perspectives to understand lake ice dynamics in a changing world. J Geophys Res-biogeo 2020; 125: e2020JG005799.

[42] Hobday AJ, Alexander LV, Perkins SE, et al. A hierarchical approach to defining marine heatwaves. Prog Oceanogr 2016; 141: 227-238.

[43] Allen M. Liability for climate change. Nature 2003; 421: 891-892.

[44] Woolway RI, Albergel C, Frölicher TL, et al. Severe lake heatwaves attributable to human-induced global warming. Geophys Res Lett 2022; 49: e2021GL097031.

[45] Zheng M. An introduction to saline Lakes on the Qinghai-Tibet plateau. Springer Science & Business Media; 1997.

[46] Sun Y, Zhang X, Zwiers FW, et al. Rapid increase in the risk of extreme summer heat in Eastern China. Nat Clim Change 2014; 4: 1082-1085.

[47] Xie C, Zhang X, Zhuang L, et al. Analysis of surface temperature variation of lakes in China using MODIS land surface temperature data. Sci Rep 2022; 12: 2415.

[48] Winslow LA, Leach TH, Rose KC. Global lake response to the recent warming hiatus. Environ Res Lett 2018; 13: 054005.

[49] Yang K, Ding B, Qin J, et al. Can aerosol loading explain the solar dimming over the Tibetan Plateau? Geophys Res Lett 2012; 39: L20710.

[50] Wen L, Lyu S, Kirillin G, et al. Air-lake boundary layer and performance of a simple lake parameterization scheme over the Tibetan highlands. Tellus A: Dyn Meteorol 2016; 68:

31091.

[51] Shi Y, Huang A, Ma W, et al. Drivers of warming in Lake Nam Co on Tibetan Plateau over the past 40 years. J Geophys Res-atmos 2022; 127: e2021JD036320.

[52] Guo L, Zheng H, Wu Y, et al. An integrated dataset of daily lake surface water temperature over the Tibetan Plateau. Earth Syst Sci Data 2022; 14: 3411-3422.

[53] Shi H, Zhang J, Zhao B, et al. Surface brightening in eastern and central China since the implementation of the Clean Air Action in 2013: Causes and implications. Geophys Res Lett 2021; 48: e2020GL091105.

[54] Shi K, Zhang Y, Zhang Y, et al. Phenology of phytoplankton blooms in a trophic lake observed from long-term MODIS Data. Environ Sci Technol 2019; 53: 2324-2331.

[55] North RP, North RL, Livingstone DM, et al. Long-term changes in hypoxia and soluble reactive phosphorus in the hypolimnion of a large temperate lake: Consequences of a climate regime shift. Glob Change Biol 2014; 20: 811-823.

[56] Jane SF, Hansen GJA, Kraemer BM, et al. Widespread deoxygenation of temperate lakes. Nature 2021; 594: 66-70.

[57] Liu M, Zhang Y, Shi K, et al. Thermal stratification dynamics in a large and deep subtropical reservoir revealed by high-frequency buoy data. Sci Total Environ 2019; 651: 614-624.

[58] Ficke AD, Myrick CA, Hansen LJ. Potential impacts of global climate change on freshwater fisheries. Rev Fish Biol Fisher 2007; 17: 581-613.

[59] Till A, Rypel AL, Bray A, et al. Fish die-offs are concurrent with thermal extremes in

north temperate lakes. Nat Clim Change 2019; 9: 637-641.

[60] Dokulil MT, de Eyto E, Maberly SC, et al. Increasing maximum lake surface temperature under climate change. Clim Change 2021; 165: 56.

[61] Woolway RI, Maberly SC. Climate velocity in inland standing waters. Nat Clim Change 2020; 10: 1124-1129.

[62] Søndergaard M, Jensen JP, Jeppesen E. Role of sediment and internal loading of phosphorus in shallow lakes. Hydrobiologia 2003; 506-509: 135-145.

[63] Gudasz C, Bastviken D, Steger K, et al. Temperature-controlled organic carbon mineralization in lake sediments. Nature 2010; 466: 478-481.

[64] Kosten S, Huszar VLM, Bécares E, et al. Warmer climates boost cyanobacterial dominance in shallow lakes. Glob Change Biol 2012; 18: 118-126.

[65] Li Y, Shang J, Zhang C, et al. The role of freshwater eutrophication in greenhouse gas emissions: A review. Sci Total Environ 2021; 768: 144582.

[66] Paerl HW, Huisman J. Blooms like it hot. Science 2008; 320: 57-58.

[67] Donis D, Mantzouki E, McGinnis DF, et al. Stratification strength and light climate explain variation in Chlorophyll *a* at the continental scale in a European multi-lake survey in a heatwave summer. Limnol Oceanogr 2021; 66: 4314-4333.

[68] Hou X, Feng L, Dai Y, et al. Global mapping reveals increase in lacustrine algal blooms over the past decade. Nat Geosci 2022; 15: 130-134.

[69] Carmichael WW, Azevedo SM, An JS, et al. Human fatalities from cyanobacteria: Chemical and biological evidence for cyanotoxins. Environ Health Perspect 2001; 109: 663-

668.

Figure 1–6

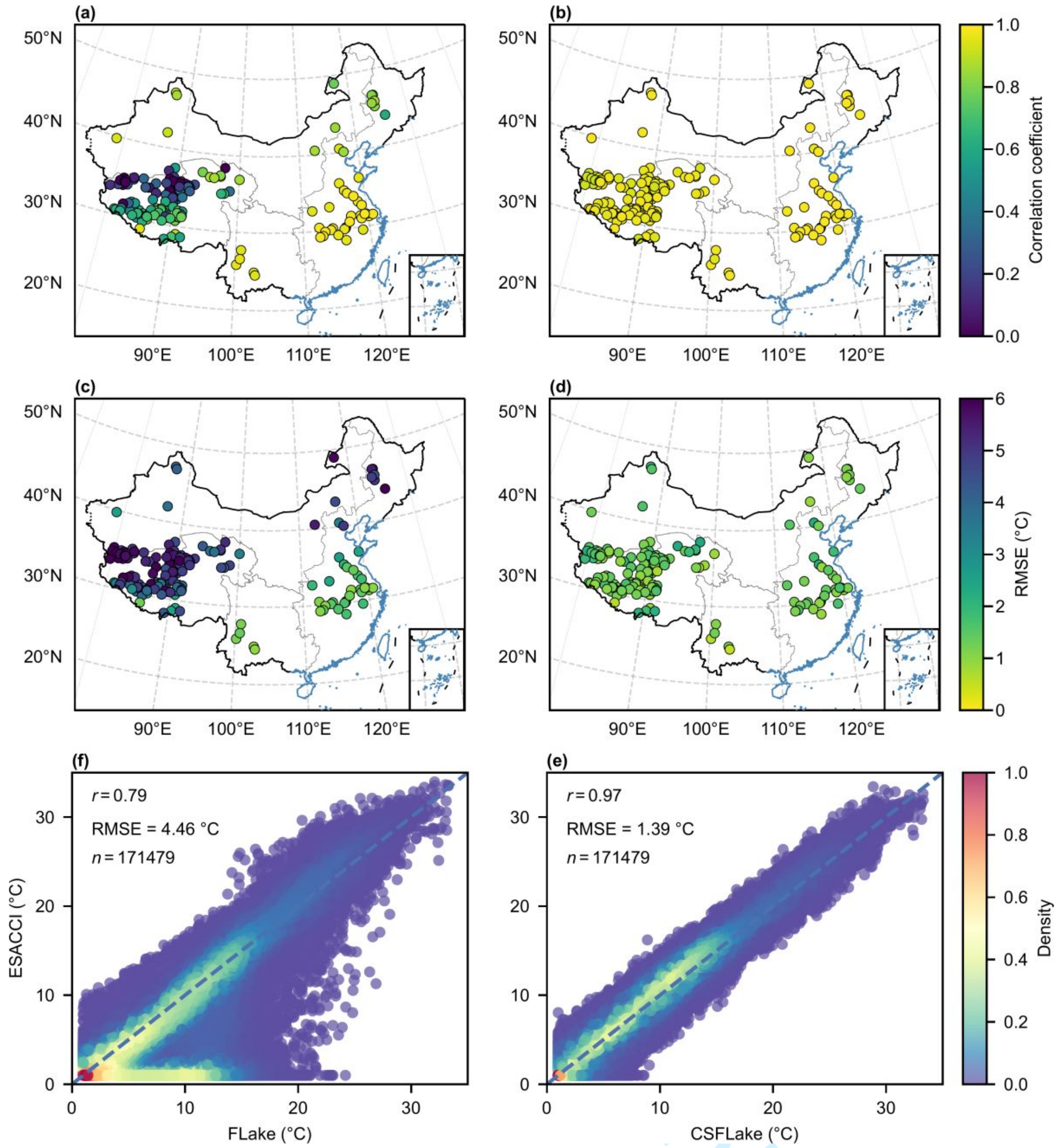

Figure 1 Validation of simulated lake surface water temperature (2000–2020). (a–b) Pearson correlation between ESACCI and FLake (a) and CSFLake (b). (c–d) Root mean square error (RMSE) between ESACCI and FLake (c) and CSFLake (d). (e–f) Comparisons between the lake surface water temperature from satellites and simulation results. (e) ESACCI versus FLake. (f) ESACCI versus CSFLake. Pearson correlation coefficient (italics "r"), RMSE, and the number of points (italics "n") are given in the text. The density of points was computed as the normalized kernel density estimation. Note that some lakes in (a) were not shown because they remained frozen (always 1 °C) during satellite data–taking period.

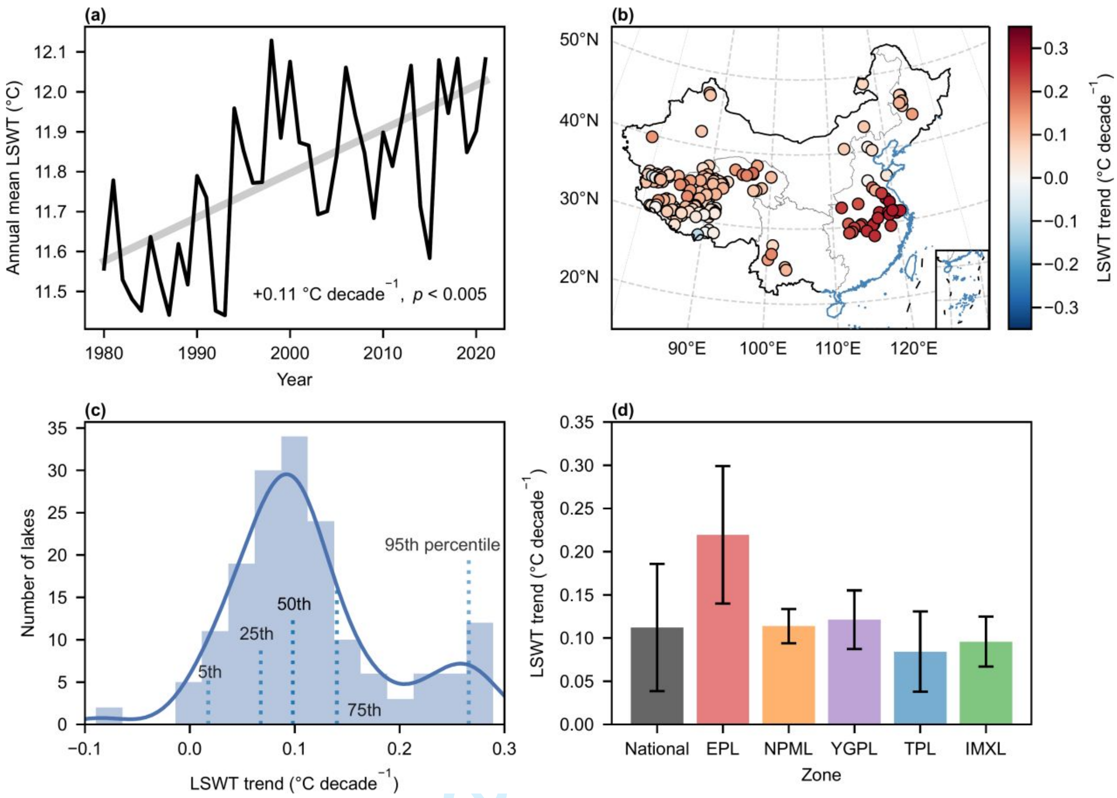

Figure 2 Trend of lake surface water temperature (1980–2021). (a) Annual mean lake surface water temperature (LSWT) averaged over all studied lakes. (b) Spatial distribution of the LSWT trends. (c) Histogram (bar), kernel density estimation (solid line), and percentiles (dashed line) of the LSWT trend. (d) The LSWT trend averaged over all lakes and five lake zones. The whiskers represent the standard deviation.

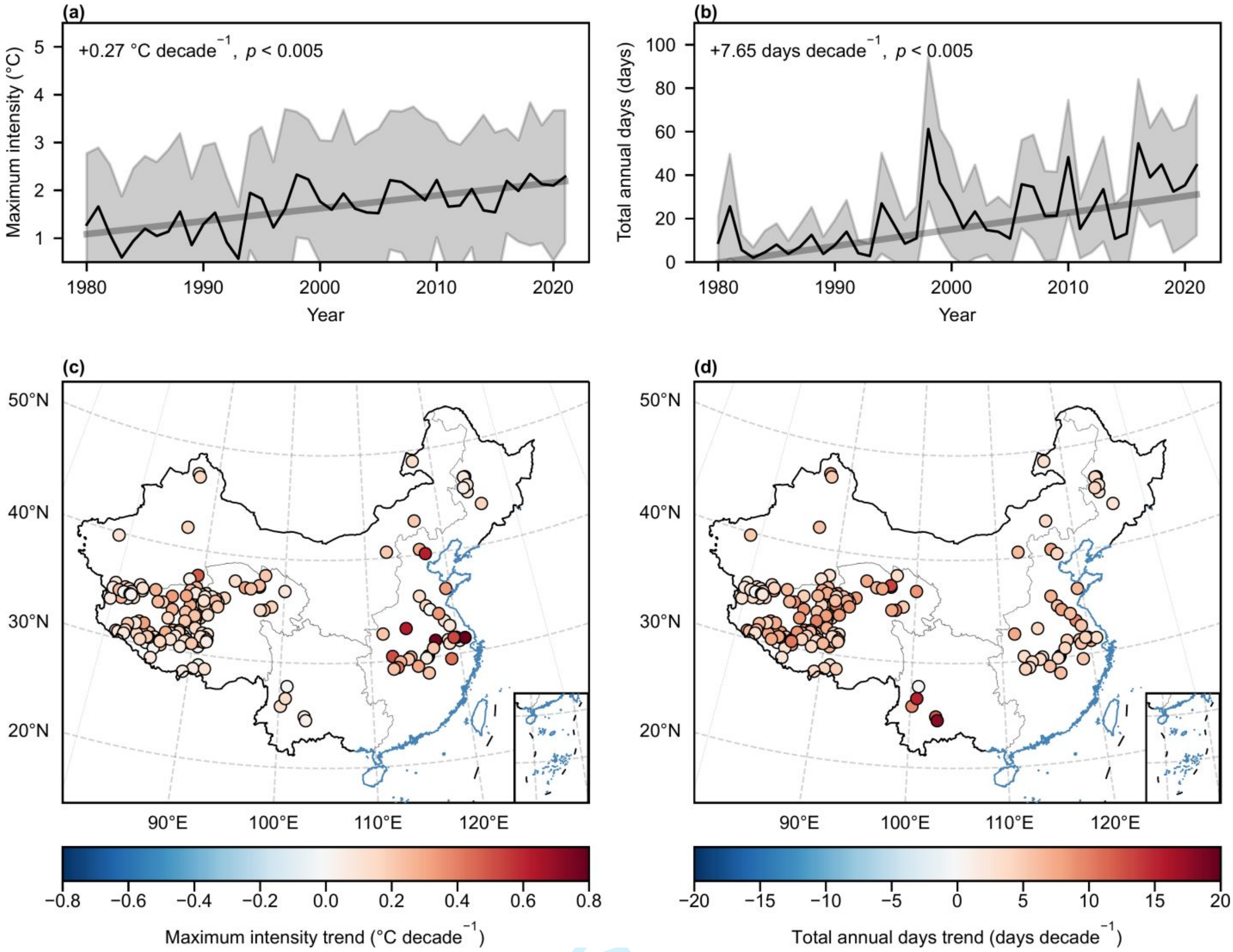

Figure 3 Lake heatwave metrics during 1980–2021. (a-b) Annual time series of averaged maximum lake heatwave intensity (a) and total annual days (b). The spatial distribution of their annual trends over 1980–2021 is shown in (c) and (d). The solid lines and shaded areas in (a–b) denote the average of all studied lakes and the standard deviation, respectively.

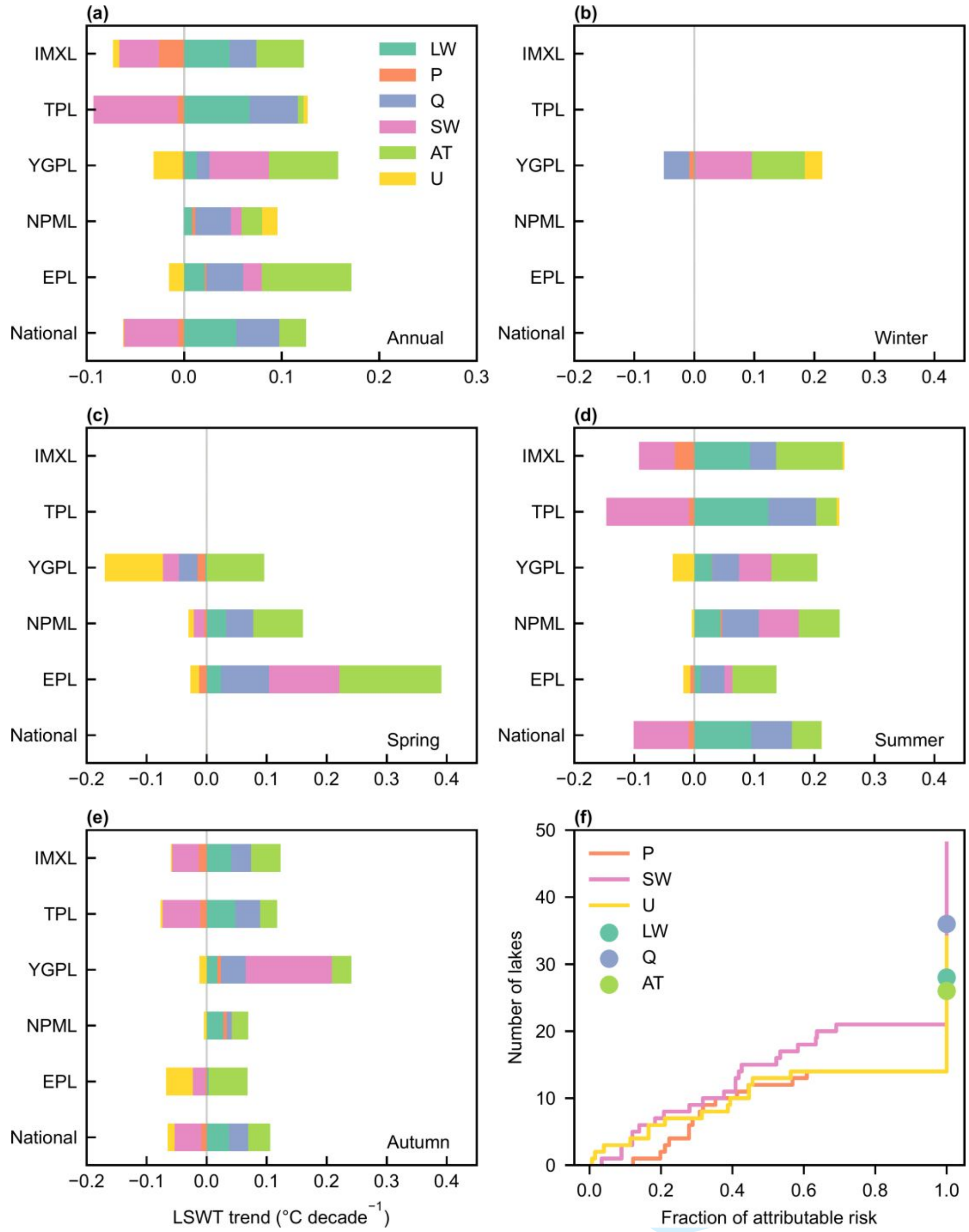

Figure 4 Contribution of meteorological variables to the trend of lake surface water temperature (LSWT; 1980–2021). (a) Contribution of surface downward longwave radiation (LW), surface pressure (P), 2 m specific humidity (Q), surface downward shortwave radiation (SW), 2 m air temperature (AT), and 10 m wind speed (U) to the LSWT trend for five lake zones. (b-e) The contribution of meteorological variables for winter (b; December, January, and February), spring (c; March, April, and May), summer (d; June, July, and August), and autumn (e; September, October, and November) to the LSWT trends. (f) Contributions of meteorological variables to the occurrence of long lake heatwaves.

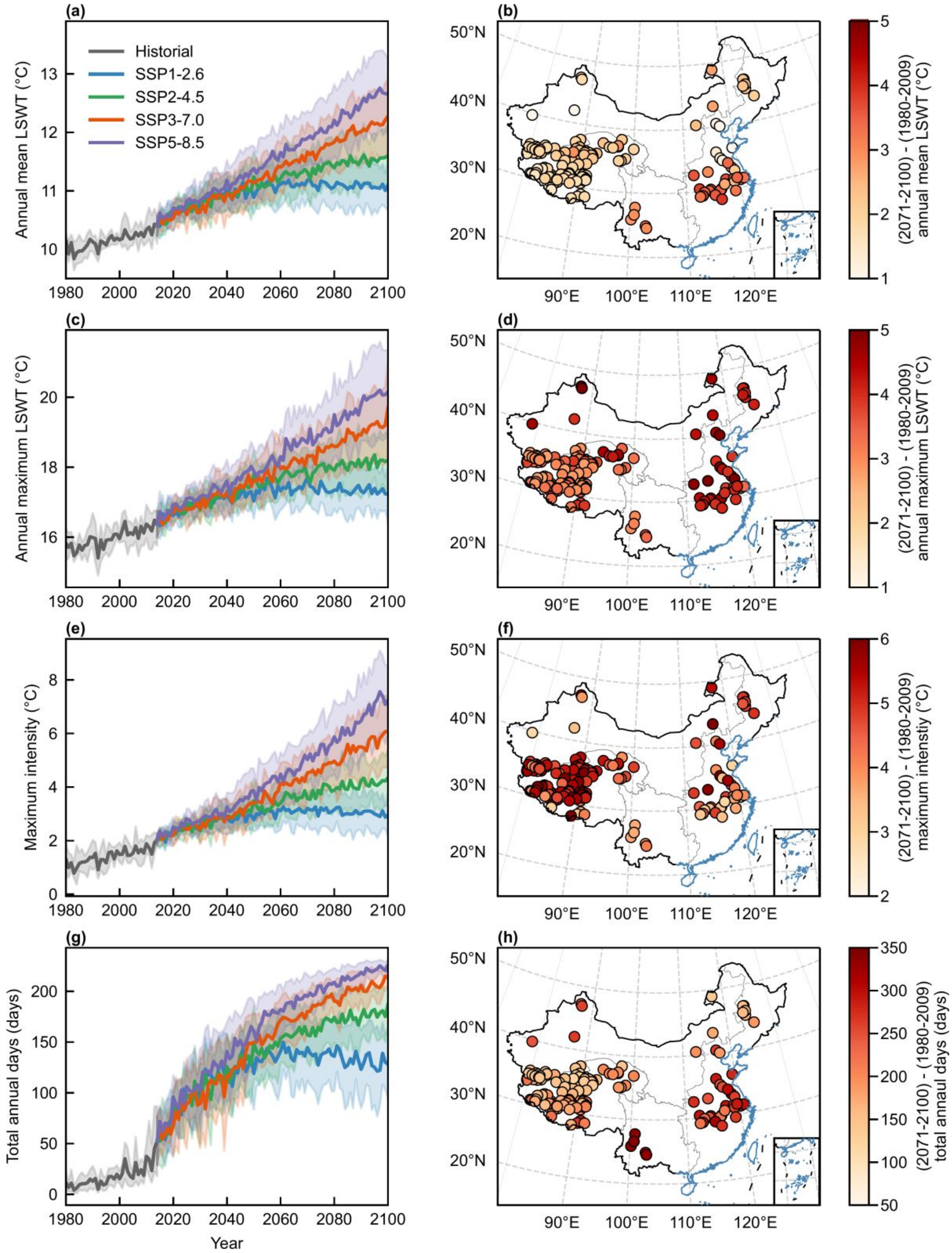

Figure 5 Future projection of lake surface water temperature and heatwaves. Temporal changes of the (a) annual mean lake surface water temperature (LSWT), (c) annual maximum LSWT, (e) annual mean lake heatwave maximum intensity, and (g) lake heatwave total annual days under historical and future climate forcing (SSP1-2.6, SSP2-4.5, SSP3-7.0, SSP5-8.5). The solid lines show the mean across all the studied lakes and five lake-climate ensembles. The shaded areas represent the standard deviation between climate ensembles. Differences between SSP5-8.5 run (averaged over 2071–2100 and five lake-climate ensembles) and historical run (averaged over 1980–2009 and five lake-climate ensembles) of the (b) annual mean LSWT, (d) annual maximum LSWT, (f) annual mean lake heatwave maximum intensity, and (h) lake heatwave total annual days.

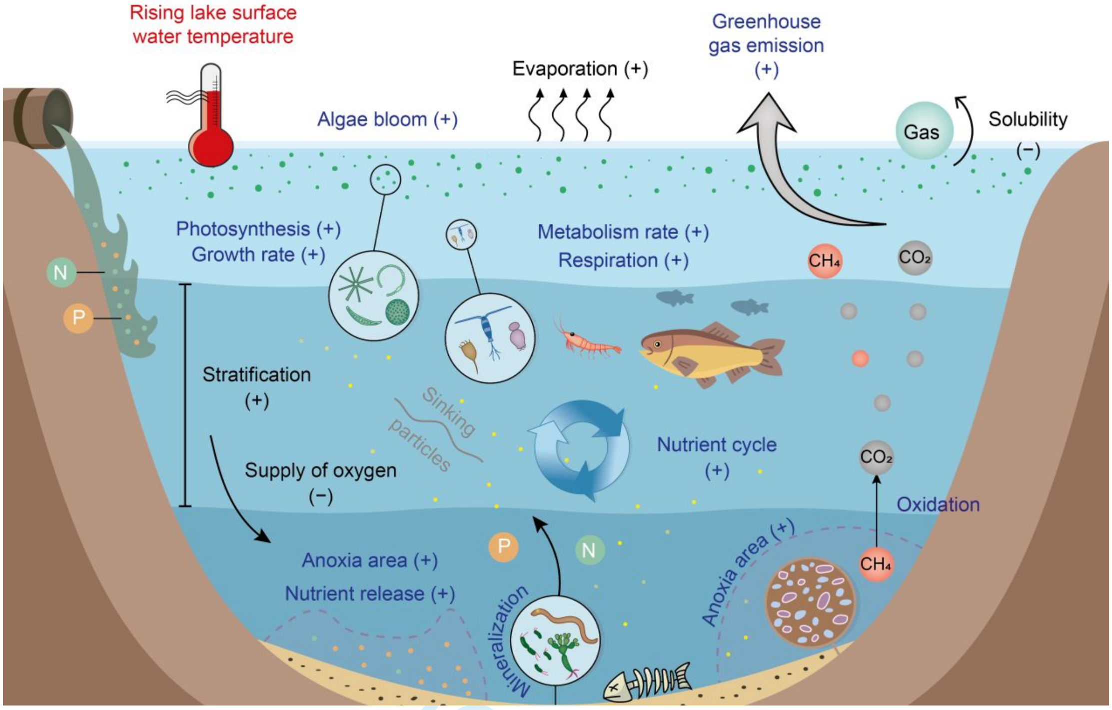

Figure 6 Implications of rising lake surface water temperature in the lake ecosystem. The biochemical and physical processes are represented by blue and black text, respectively. The symbol “+” after the name of a process indicates that increases in lake surface water temperature may facilitate the process, while “−” indicates the opposite. The absence of a symbol means the effect of rising lake surface water temperature on this process is unclear.

Supplementary Materials to "Climate change drives rapid warming and increasing heatwaves of lakes"

Xiwen Wang[a, b], Kun Shi[a, c, d, *], Yunlin Zhang[a, c, d, *], Boqiang Qin[a], Yibo Zhang[a], Weijia Wang[a, c, d], R. Iestyn Woolway[e], Shilong Piao[f–h], Erik Jeppesen[i–l]

[a] Taihu Laboratory for Lake Ecosystem Research, State Key Laboratory of Lake Science and Environment, Nanjing Institute of Geography and Limnology, Chinese Academy of Sciences, Nanjing 210008, China

[b] Key Laboratory of Western China's Environmental Systems (Ministry of Education), College of Earth and Environmental Sciences, Lanzhou University, Lanzhou, 730000, China

[c] University of Chinese Academy of Sciences, Beijing 100049, China

[d] College of Nanjing, University of Chinese Academy of Sciences, Nanjing 2111, China

[e] School of Ocean Sciences, Bangor University, Menai Bridge, Anglesey, UK

[f] Sino-French Institute for Earth System Science, College of Urban and Environmental Sciences, Peking University, Beijing, China

[g] Key Laboratory of Alpine Ecology, Institute of Tibetan Plateau Research, Chinese Academy of Sciences, Beijing, China

[h] Center for Excellence in Tibetan Earth Science, Chinese Academy of Sciences, Beijing, China

[i] Department of Ecoscience, Aarhus University, Aarhus C, 8000, Denmark

[j] Sino-Danish Centre for Education and Research, Beijing, China

[k] Limnology Laboratory, Department of Biological Sciences and Centre for Ecosystem Research and Implementation (EKOSAM), Middle East Technical University, Ankara, 06800, Türkiye

[l] Institute of Marine Sciences, Middle East Technical University, Erdeneli-Mersin, 33731, Turkey

***Corresponding author**: Kun Shi and Yunlin Zhang, Nanjing Institute of Geography and Limnology, Chinese Academy of Sciences, 73 East Beijing Road, Nanjing 210008, P. R. China, Tel: + 86-25-86882008, Email: kshi@niglas.ac.cn, ylzhang@niglas.ac.cn

Supplementary Figures and Tables

Figure S1-18

Table S 1-2

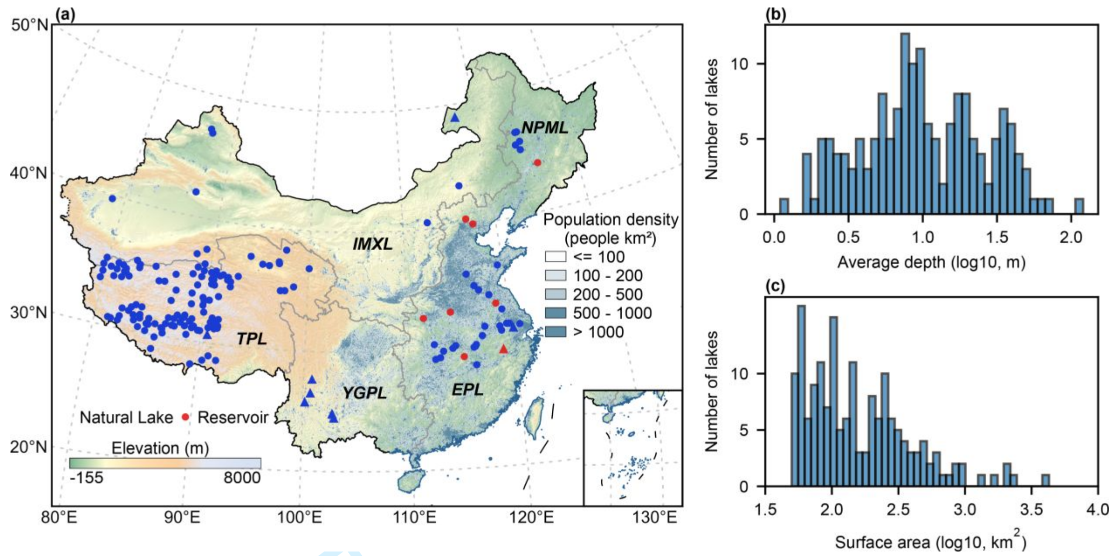

Figure S1 Distribution and characteristics of the studied lakes. (a) Map of the studied natural lakes and artificial reservoirs. (b) Histograms of log10[surface area (km^2)]. (c) Histograms of log10[average depth (m)]. The information is derived from the HydroLAKES database. The location of lake points is the centroids of lake polygons. The triangles in (a) represent the nine lakes on which ground observations are available for model verification. The population density dataset is derived from WorldPop (www.wordpop.org).

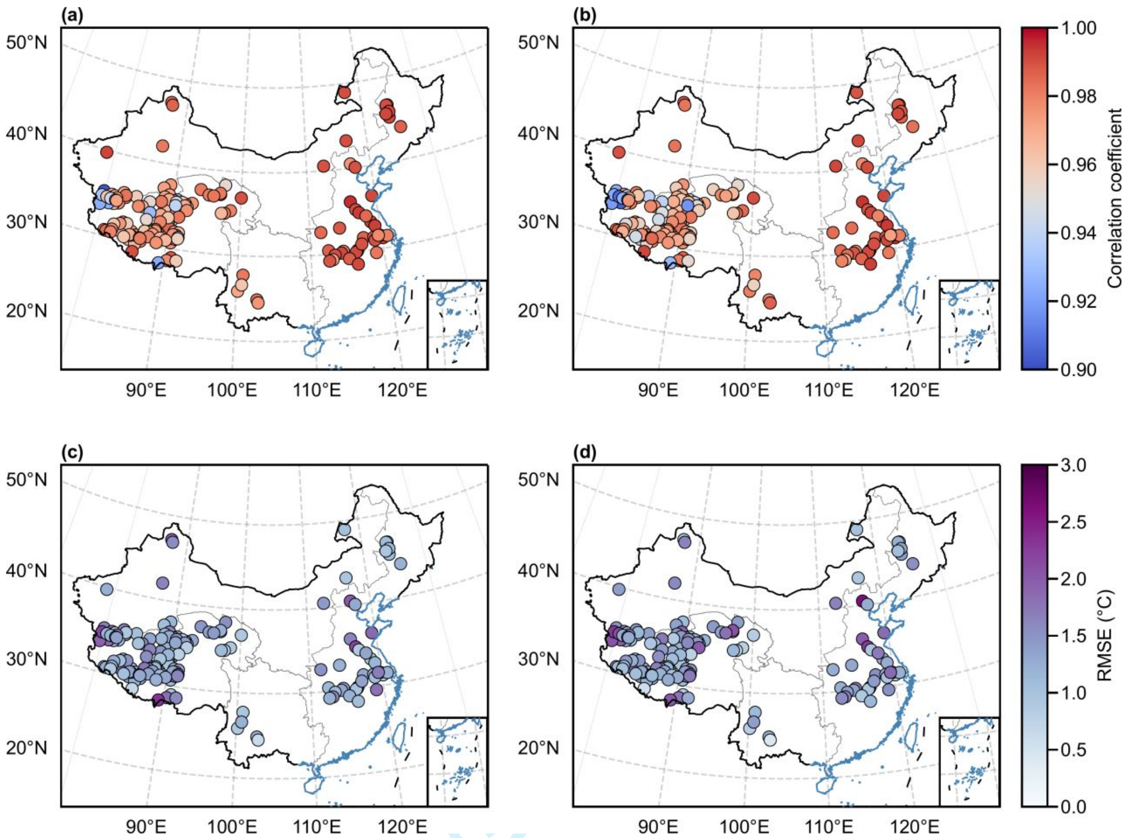

Figure S2 Model performances during 2001–2010 (calibration phase) and 2011–2020 (verification phase). (a-b) Pearson correlation coefficient between simulation results and ESACCI during 2001–2010 (a) and 2011–2020 (b). (c-d) Root mean square error (RMSE; unit: °C) between simulation results and ESACCI during 2001– 2010 (c) and 2011–2020 (d).

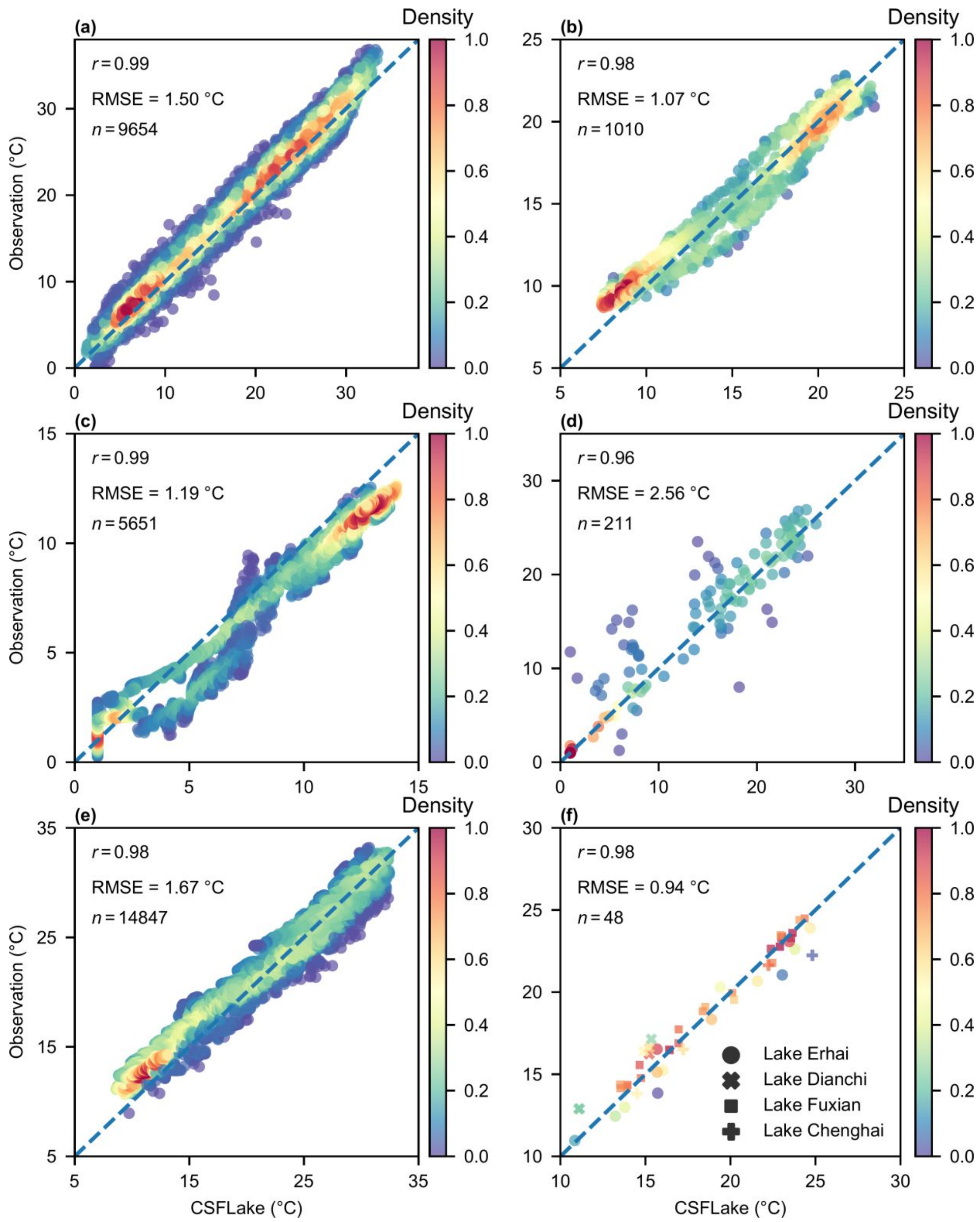

Figure S3 Comparison between the simulated lake surface water temperature using CSFLake and observations. (a) Lake Taihu. (b) Lake Lugu. (c) Lake Namco. (d) Lake Hulun. (e) Lake Qiandao. (f) Four lakes on the Yunnan-Guizhou plateau. The Pearson correlation coefficient (italics "r"), root mean square error (RMSE), and the number of points (n) are shown in the text. The density of points was computed as the normalized kernel density estimation.

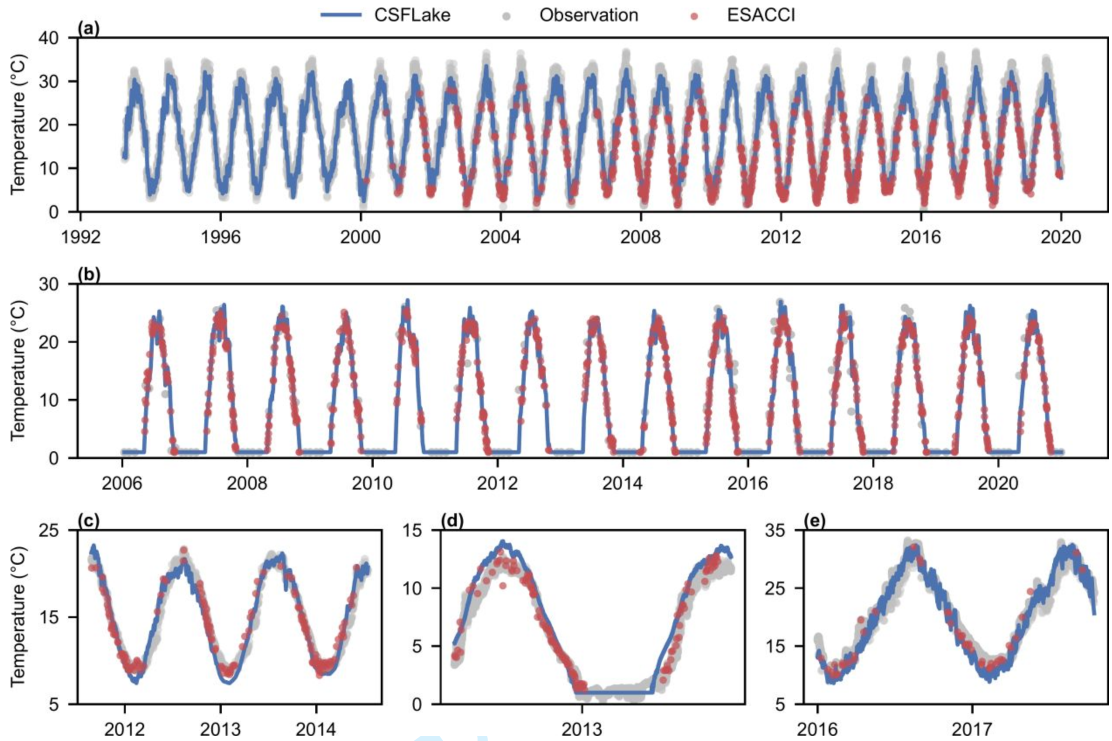

Figure S4 Comparison of lake surface water temperature between CSFLake, ESACCI, and ground observations. (a) Lake Taihu. (b) Lake Hulun. (c) Lake Lugu. (d) Lake Namco. (e) Lake Qiandao.

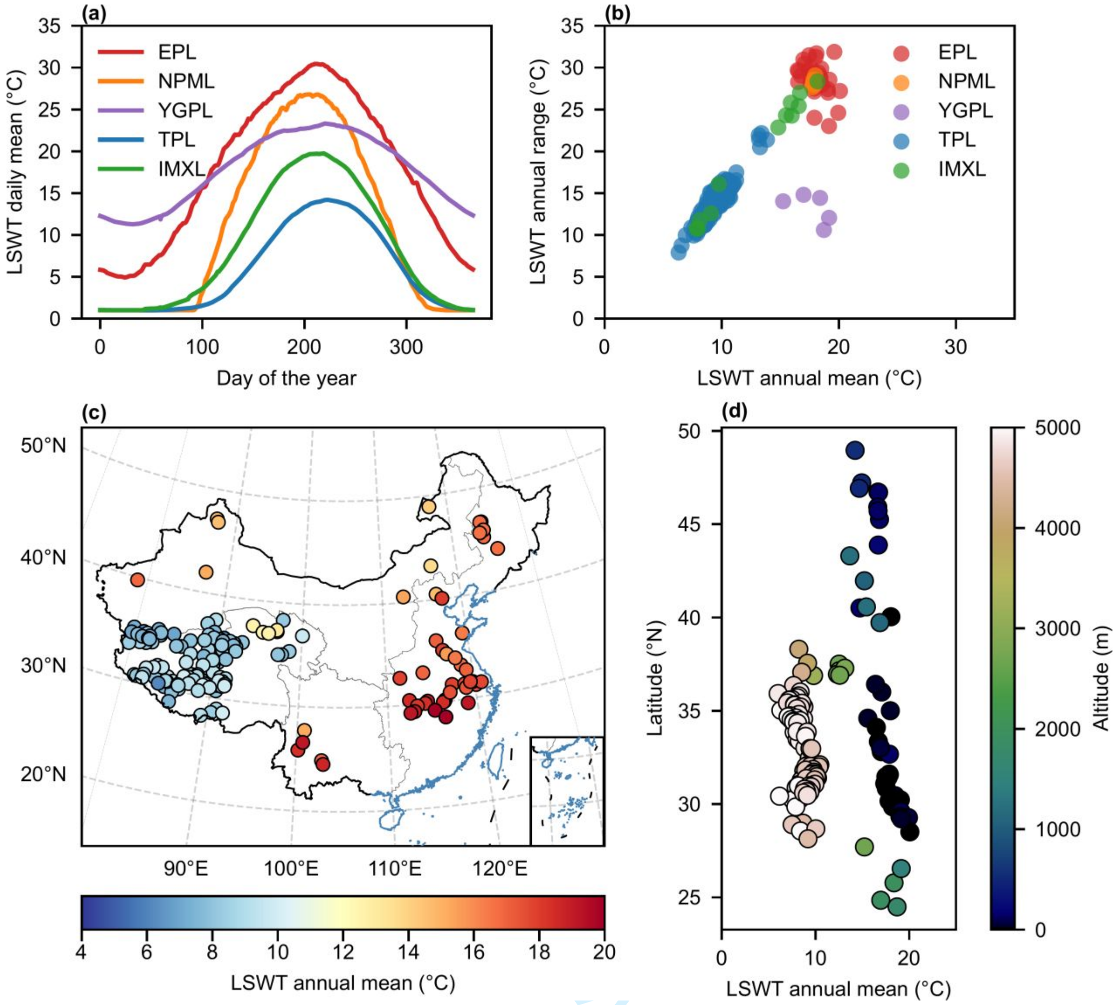

Figure S5 Climatological daily mean, annual mean, and annual range of lake surface water temperature. (a) Climatological daily mean lake surface water temperature (LSWT) for each day of the year from 1980 to 2021 in five lake zones. (b) Average of LSWT annual mean vs. annual range from 1980 to 2021 in five lake zones. The annual range was calculated by annual maximum minus annual minimum surface water temperatures. (c) Spatial distribution of the climatological annual mean LSWT for each year from 1980 to 2021 and (d) its variation across latitudes and altitudes.

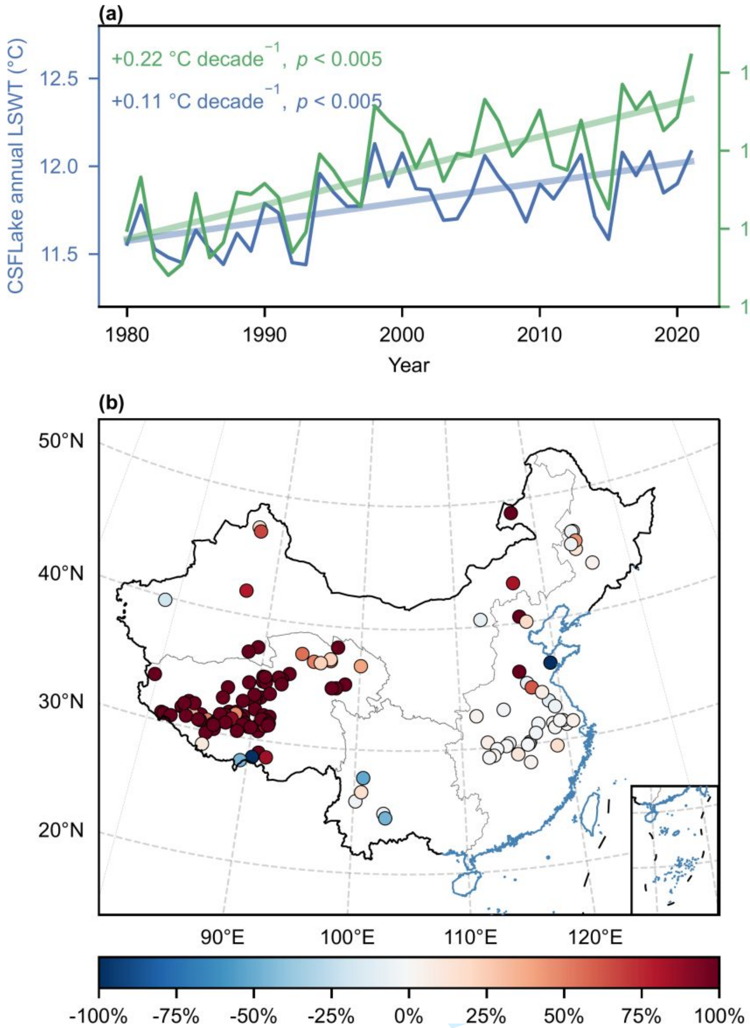

Figure S6 Comparison of the LSWT trends simulated by CSFLake and FLake. (a) Annual mean LSWT and trend of all studied lakes. (b) Percent errors between the LSWT trends simulated by CSFLake and FLake. Percent error = (T − E) / T × 100, where T and E denote the LSWT trend simulated by CSFLake and FLake, respectively. Note that some lakes are not shown in the figures because they stayed frozen for at least one year and their trends were therefore not calculated.

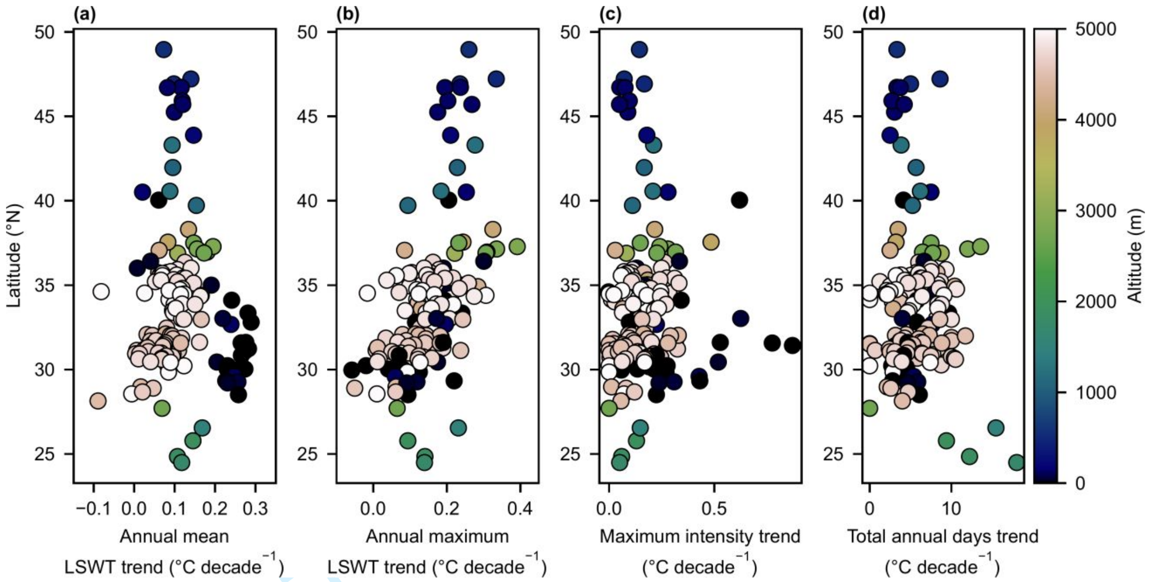

Figure S7 Variations along latitude and altitude (1980–2021). (a) Annual mean lake surface water temperature (LSWT) trend. (b) Annual maximum LSWT trend. (c) Lake heatwave (LHW) maximum intensity trend. (d) LHW total annual days trend.

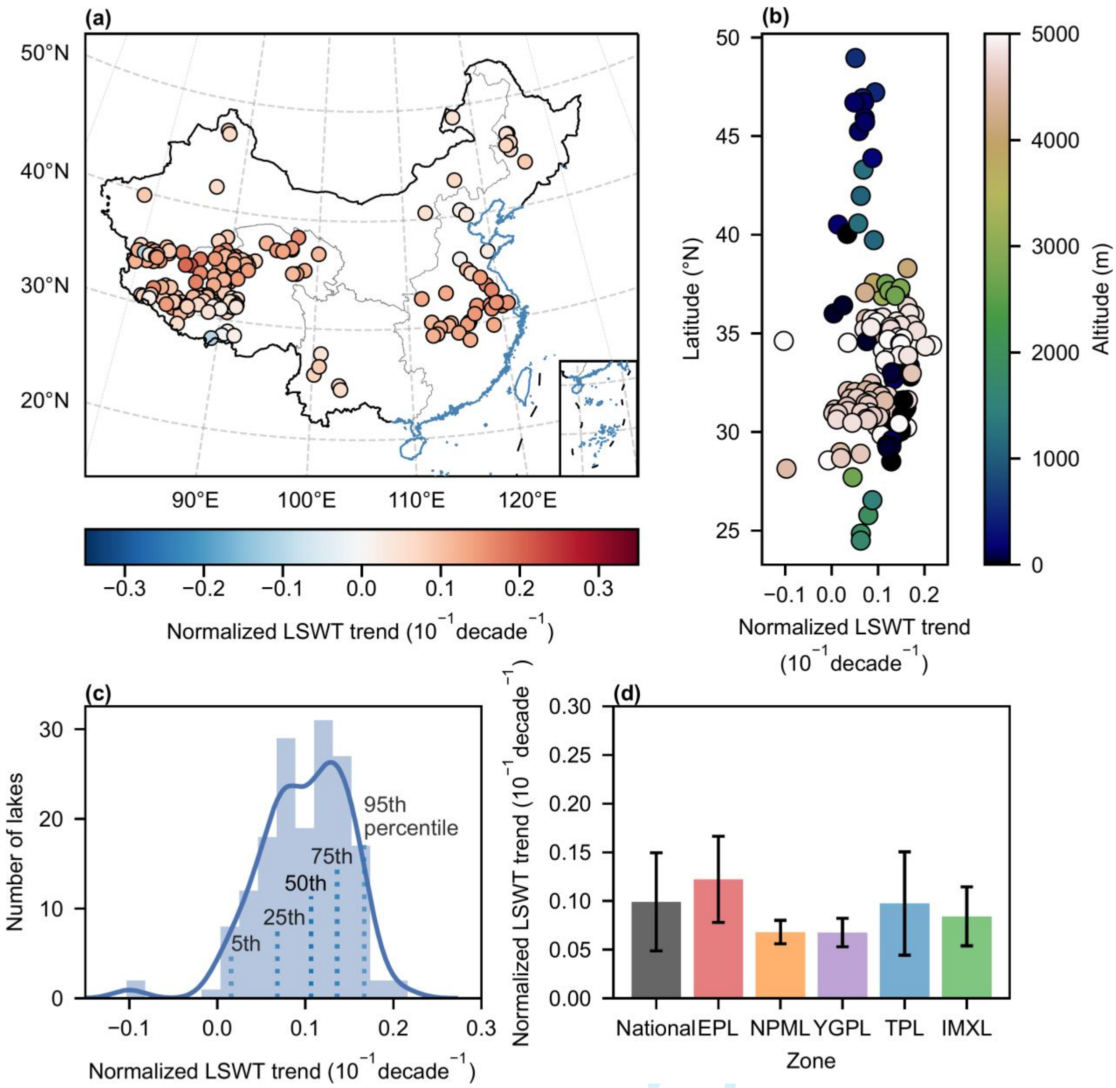

Figure S8 Normalized trend of lake surface water temperature (1980–2021). Same as Figure 2 but the trend of lake surface water temperature is normalized by its annual mean climatology from 1980 to 2021.

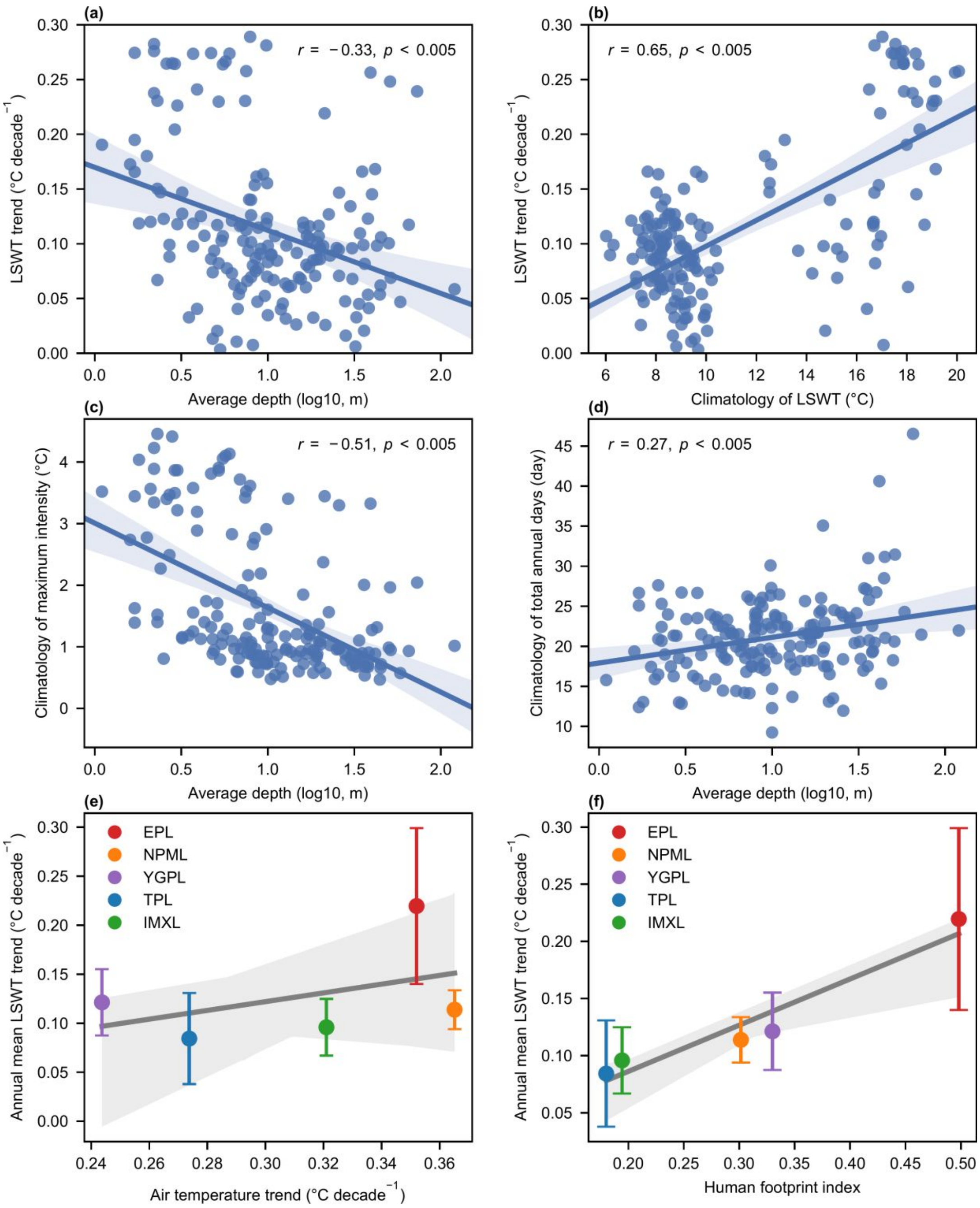

Figure S9 Relationships between lake characteristics and lake water temperature. (a–b) Lake surface water temperature (LSWT) trend versus average depth (a) and annual mean climatology of LSWT (b; 1980–2021). (c–d) Lake average depth versus the annual mean climatology of lake heatwave maximum intensity (c) and total annual days (d). Each point represents a value from one lake. Italics "r" and "p" denote the Pearson correlation coefficient and its significance. (e–f) The relationship between LSWT trend and air temperature trend (e) and human footprint index (f). The solid lines and their surrounding shaded areas show the linear regression model fit and 95% confidence interval, respectively.

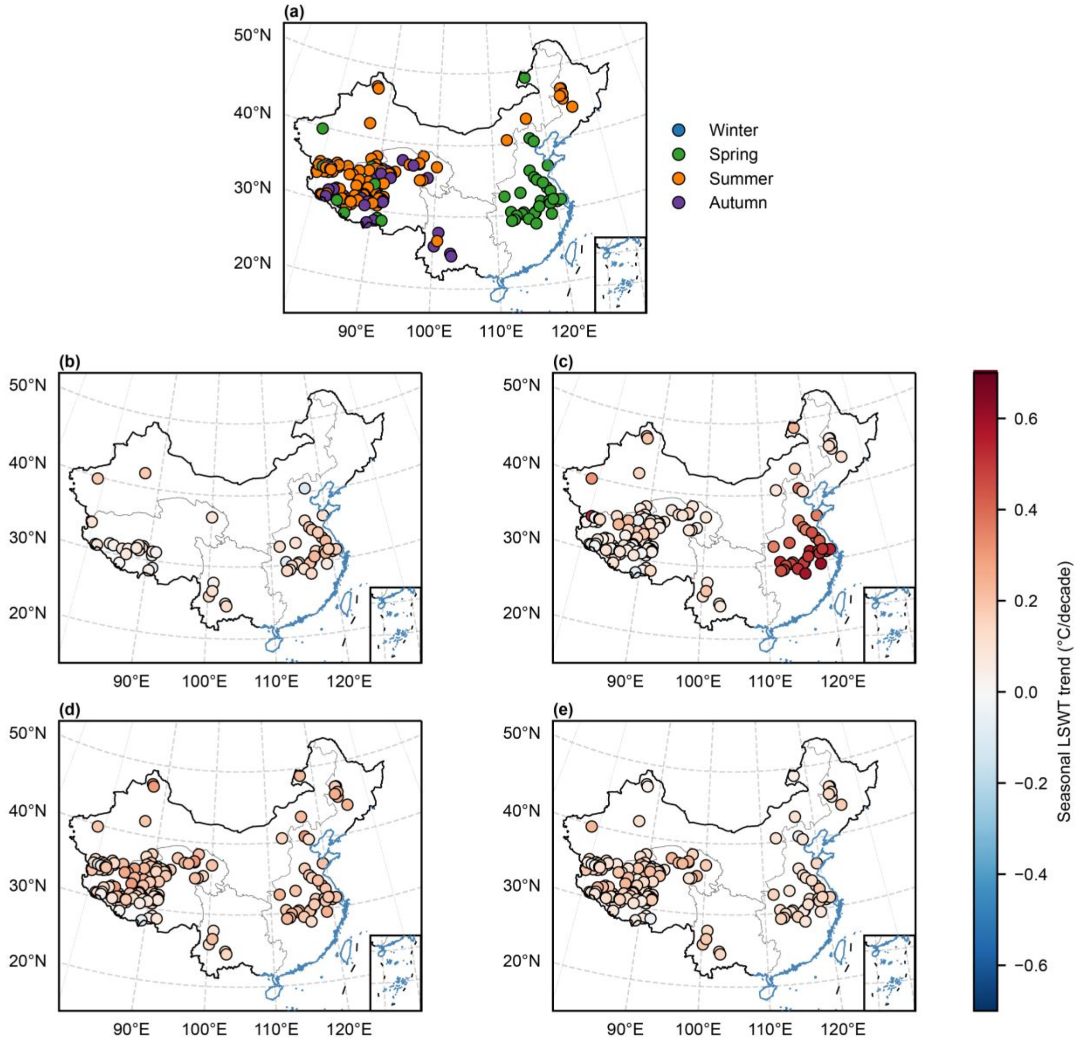

Figure S10 Trend of seasonal LSWT. (a) The fastest warming season. (b-e) The trend of LSWT in winter (b), spring (c), summer (d), and autumn (e).

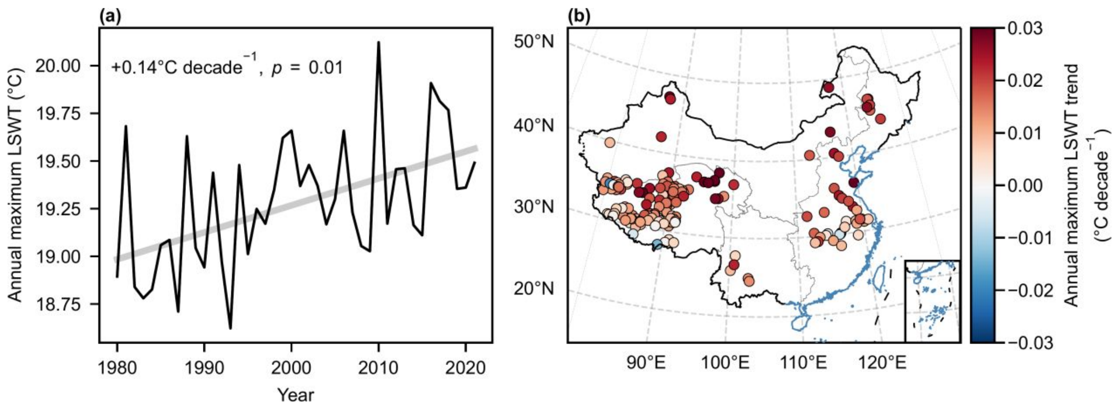

Figure S11 Annual maximum lake surface water temperature. (a-b) The trend of annual maximum lake surface water temperature (LSWT) averaged over all studied lakes (a) and its spatial distribution (b). The annotations in the top left corner show the slope and p value.

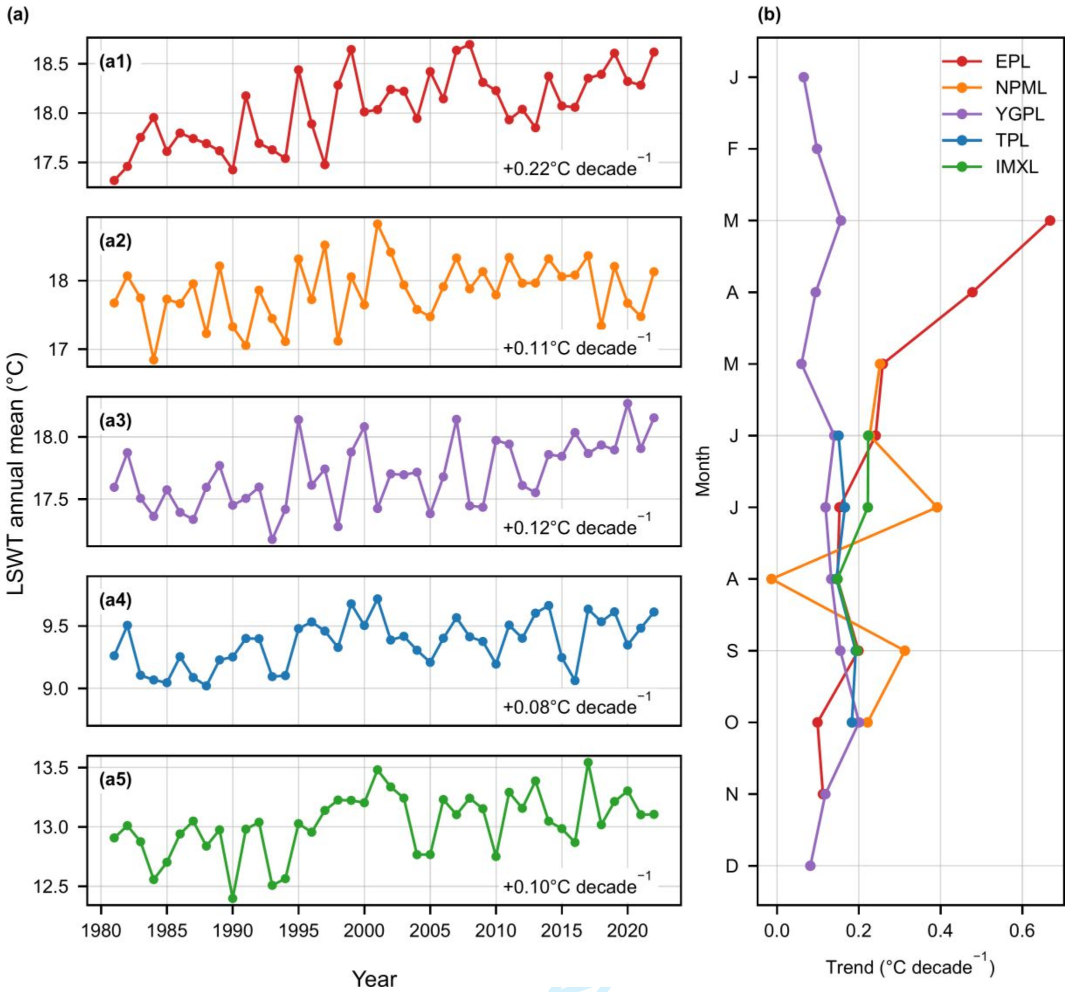

Figure S12 Variation of lake surface water temperature at different time scales. (a) Interannual variation of lake surface water temperature (LSWT) in EPL (a1), NPML (a2), YGPL (a3), TPL (a4), and IMXL (a5). (b) Monthly variation of LSWT. The solid lines in (a–b) denote the annual mean LSWT across the five lake zones.

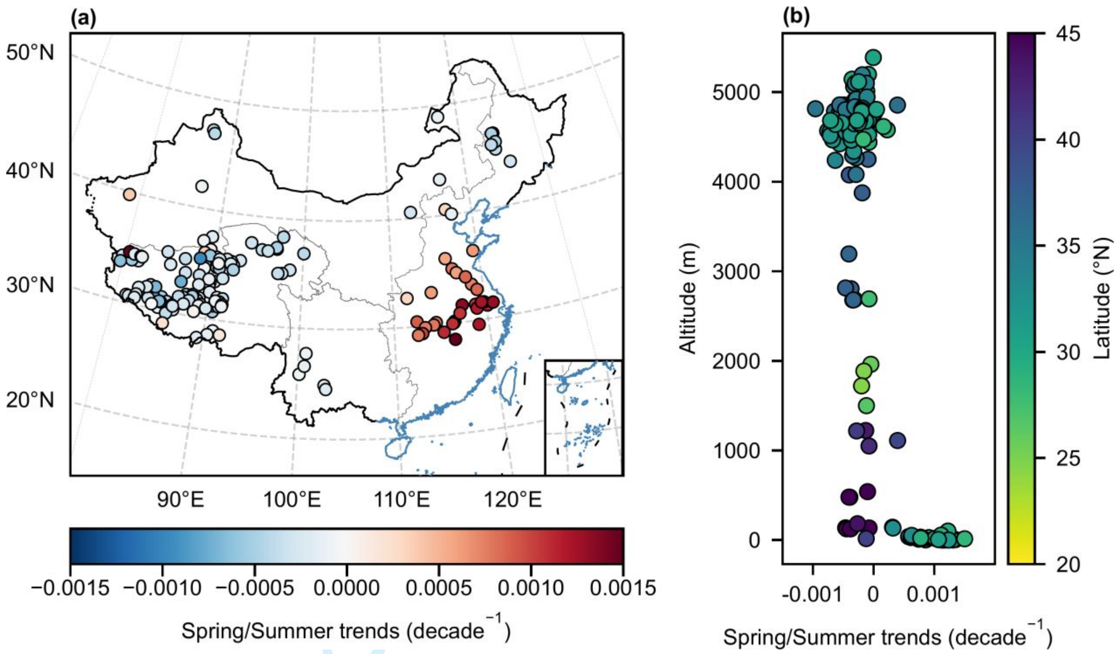

Figure S13 Trends of the ratio of spring to summer lake surface water temperature. (a) The spatial distribution. (b) The variations along altitude and latitude.

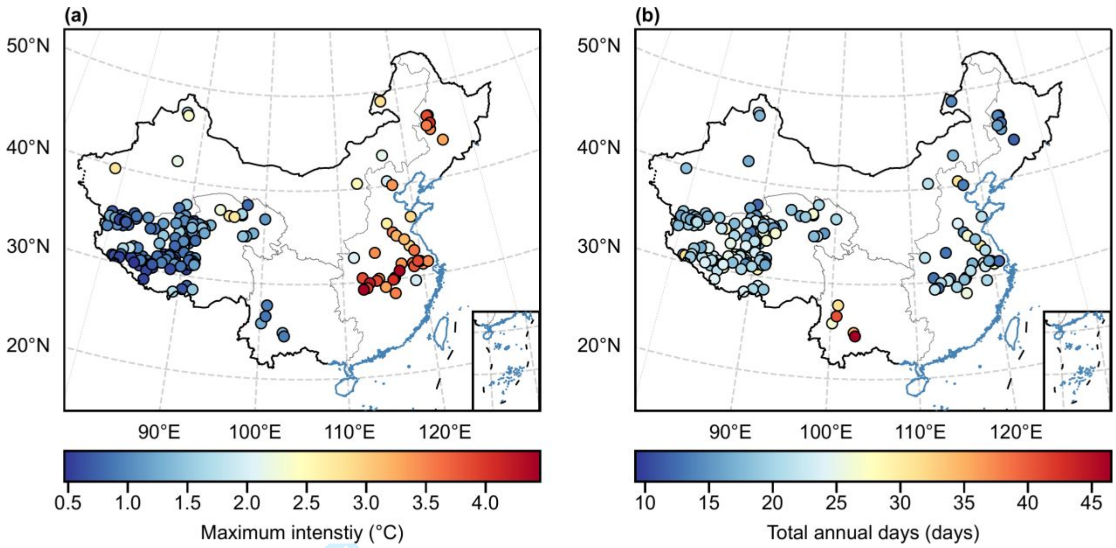

Figure S14 Lake heatwave climatology during 1980–2021. (a) The climatological mean during 1980–2021 of lake heatwave maximum intensity. (b) The climatological mean during 1980–2021 of lake heatwave total annual days.

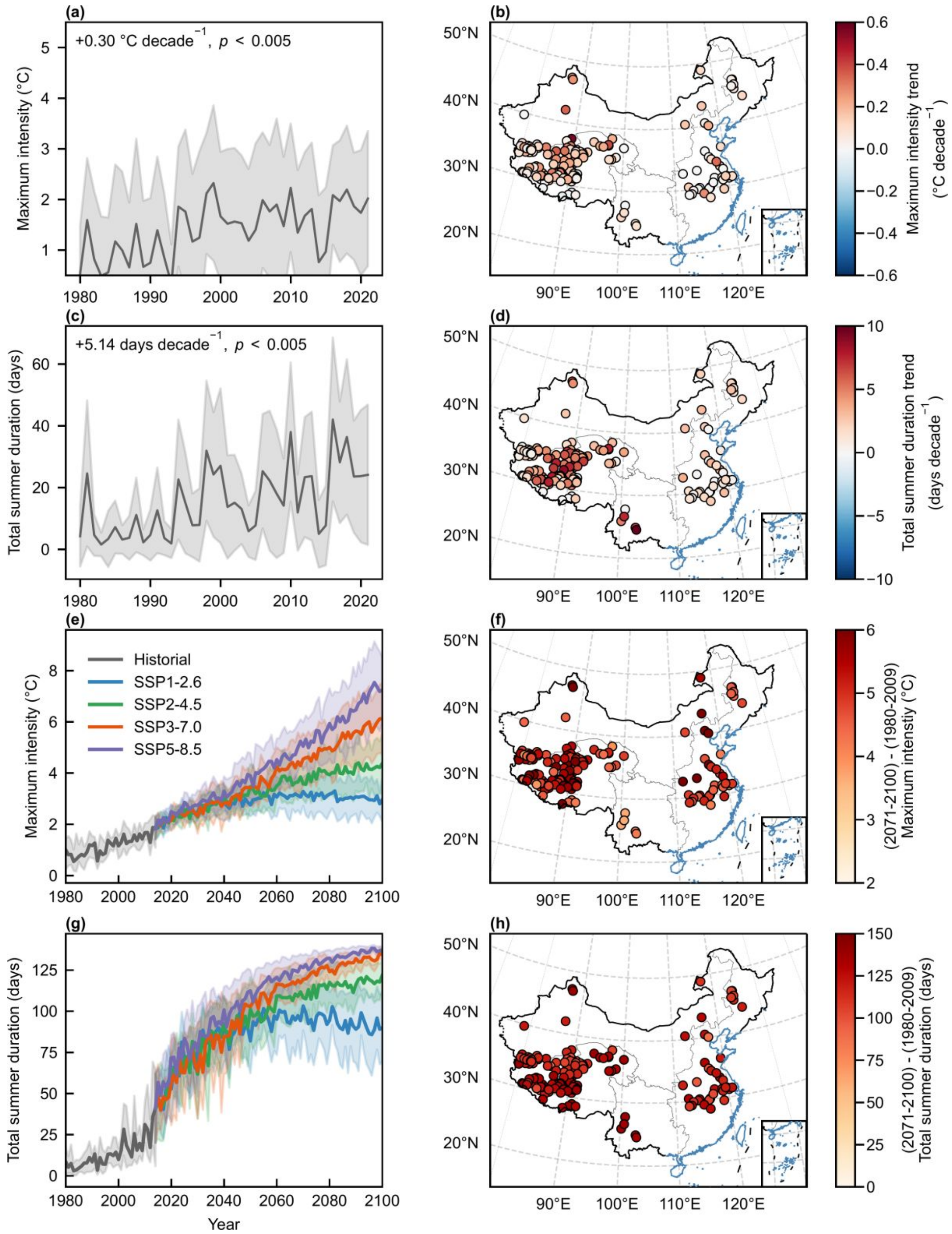

Figure S15 Historical and future projection of the warm-season (May–September) lake heatwave (1980–2100). (a-b) Annual mean (a) and climatology (b; 1980–2021) of the maximum intensity averaged over all studied lakes. (c-d) Annual mean (c) and climatology (d) of the total annual days averaged over all studied lakes. (e-f) Future projection (e) and the differences between 2071–2100 and 1980–2009 under the SSP5-8.5 scenario (f) of the maximum intensity. (g-h) Future projection (g) and the differences between 2071–2100 and 1980–2009 under the SSP5-8.5 scenario (h) of the total annual days. The solid lines and their surrounding shaded areas represent the ensemble mean and standard deviation of the simulation results driven by five global circulation models, respectively. The upper-right texts in (a) and (c) show the trend calculated using the Theil-Sen estimator and its significance.

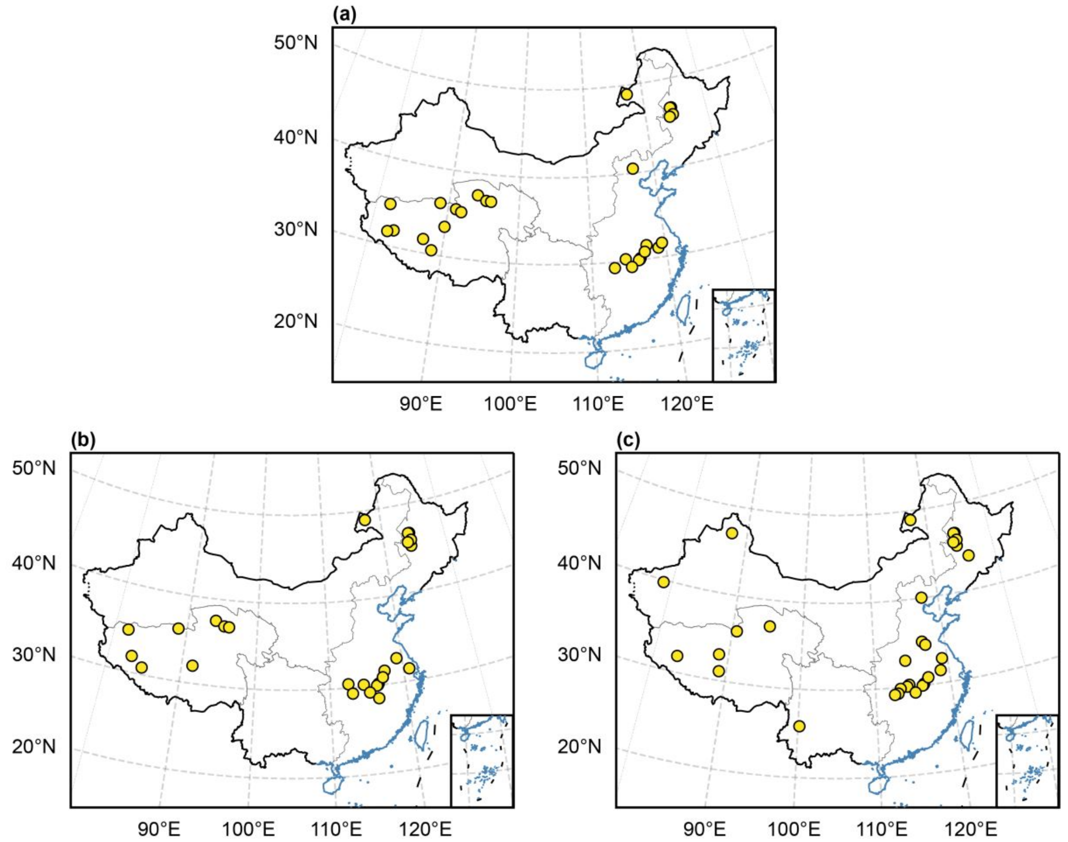

Figure S16 Lakes with a fraction attributable risk equals one. (a) Longwave radiation. (b) Specific humidity. (c) Air temperature.

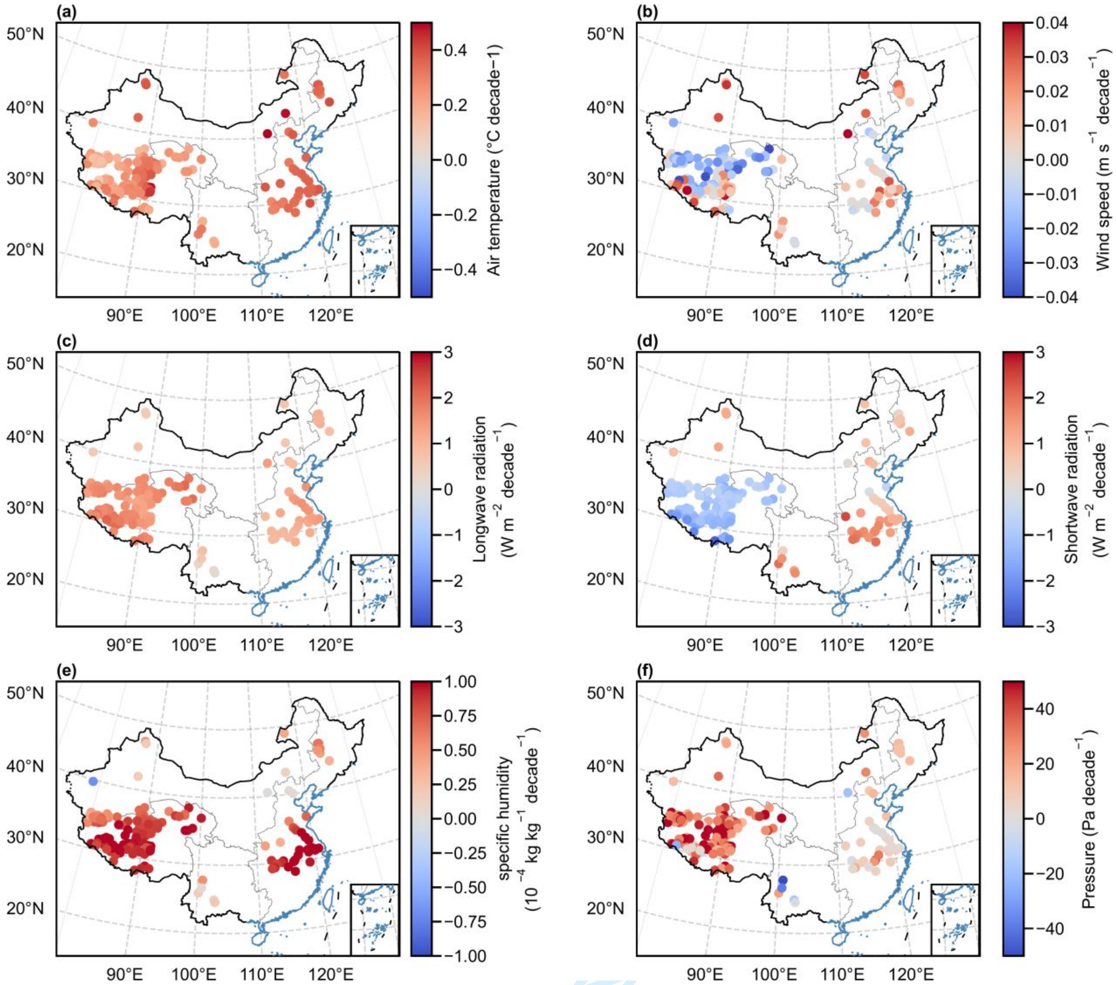

Figure S17 Trend of meteorological variables (1980–2021). (a) 2 m air temperature. (b) 10 m wind speed. (c) Surface downward longwave radiation. (d) Surface downward shortwave radiation. (e) 2 m specific humidity. (f) Surface pressure.

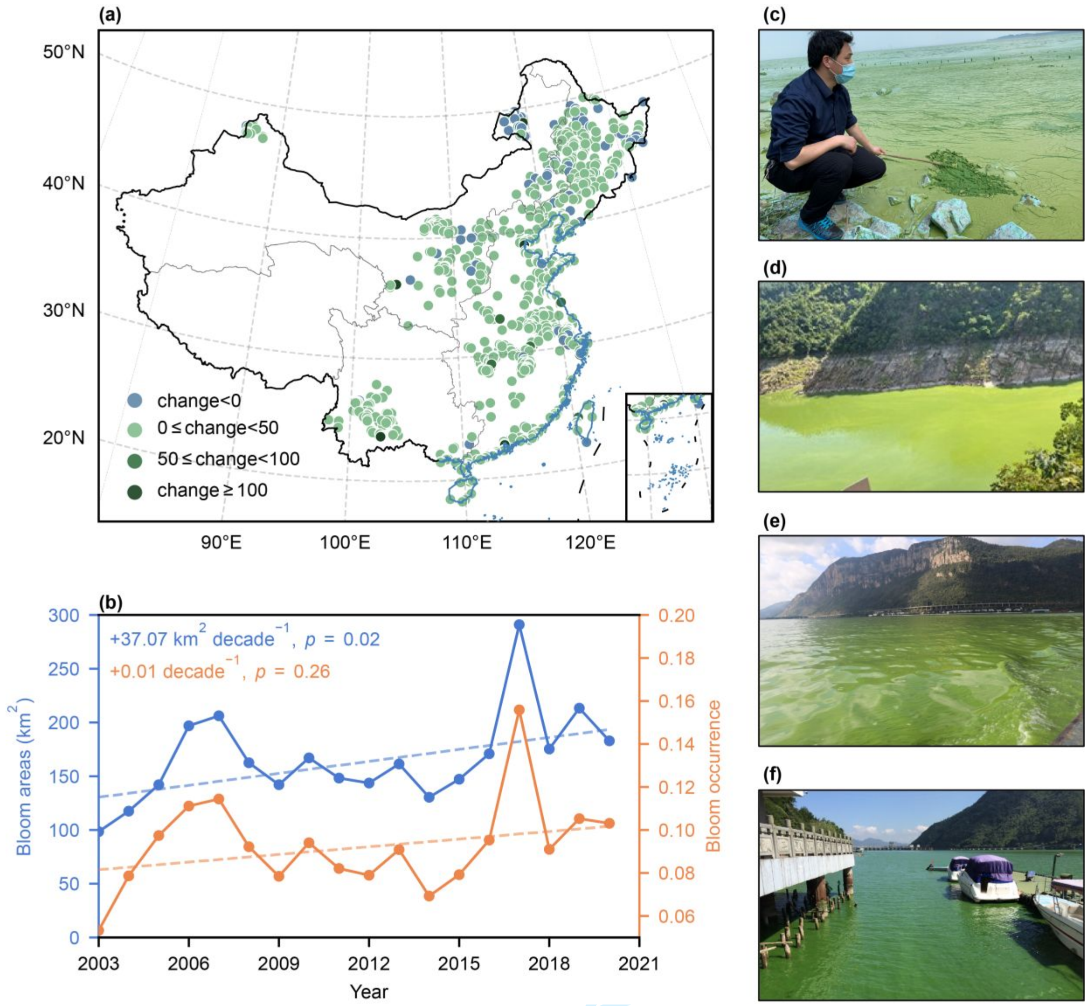

Figure S18 Algae blooms in Chinese lakes. (a) The changes in the bloom occurrence between the 2010s and 1980–1990s [1]. “change” was calculated as $(BO_{2010s} - BO_{1980–1990s}) / BO_{1980–1990s}$, where BO_x denotes the bloom occurrence during the period x. (b) The bloom areas and occurrence from 2003 to 2020 in Lake Taihu were derived from MODIS images [2]. (c–f) Photographs of algae blooms in May 2020 in Lake Taihu (c), in August 2022 in Three Gorges Reservoir (d), in October 2015 in Lake Dianchi (e), and in August 2016 in Fuchunjiang Reservoir (f).

139 Table S1 Nine lakes with ground observations.

Lake Name	ID	Temporal frequency	Thermal regime	**Lake zone**	**Surface area (km^2)**	**Average depth (m)**
Lake Taihu	148	Daily	Warm polymictic	EPL	2329.14	2.20
Lake Lugu	15431	Daily	Warm monomictic	YGPL	50.03	51.30
Lake Namco	149	Two-hourly	Dimictic	TPL	1963.82	44.40
Lake Hulun	123	Monthly	Cold polymictic	IMXL	2121.43	6.20
Lake Qiandao	1467	Hourly	Warm monomictic	EPL	424.57	50.90
Lake Erhai	1479	Irregular	Warm polymictic	YGPL	242.26	40.00
Lake Dianchi	1483	Irregular	Warm polymictic	YGPL	298.34	19.70
Lake Fuxian	1485	Irregular	Warm monomictic	YGPL	215.37	65.30
Lake Chenghai	15455	Irregular	Warm monomictic	YGPL	74.75	41.70

Table S2 Information on the studied lakes and selected best parameters. Lake ID is the ID in the HydroLAKES database. Lake type=1 or 3 represent natural lakes and lake type=2 represent reservoirs. The nine lakes that provided ground lake surface water temperature for model verification are emphasized in italics.

Lake ID	Lake type	Lake zone	Surface area (km^2)	Average depth (m)	Elevation (m)	Latitude	Longitude	Light extinction coefficient (m^{-1})	Ice albedo	Depth factor
123	*1*	*IMXL*	*2121.43*	*6.20*	*540*	*48.96*	*117.41*	*0.58*	*0.20*	*0.59*
143	1	TPL	4266.55	16.80	3194	36.89	100.05	0.24	0.25	1.02
145	2	EPL	1374.36	9.80	10	33.35	118.77	0.38	0.18	0.49
147	1	TPL	1749.53	28.00	4539	31.79	88.95	0.28	0.13	0.77
148	*1*	*EPL*	*2329.14*	*2.20*	*0*	*31.24*	*120.14*	*0.55*	*0.47*	*1.93*
149	*1*	*TPL*	*1963.82*	*44.40*	*4724*	*30.72*	*90.59*	*0.16*	*0.28*	*0.65*
1245	1	IMXL	854.89	8.00	478	47.22	87.21	0.17	0.15	1.13
1250	1	IMXL	165.81	20.90	479	46.93	87.45	0.52	0.14	0.92
1252	1	NPML	132.18	6.90	135	46.72	124.37	1.79	0.16	0.31
1257	1	NPML	429.94	5.20	136	46.71	124.17	1.75	0.14	0.30
1286	1	NPML	246.95	2.70	126	45.25	124.30	1.13	0.14	1.00
1300	1	IMXL	213.64	7.70	1223	43.30	116.65	0.54	0.20	0.80
1304	1	IMXL	961.84	9.10	1050	41.97	87.05	2.65	0.13	1.24
1317	2	EPL	121.66	36.00	143	40.51	116.89	1.86	0.25	0.71
1323	2	EPL	118.62	13.10	16	40.04	117.57	1.75	0.14	0.30
1325	1	IMXL	102.82	8.40	1111	39.73	78.73	1.61	0.20	0.38
1336	1	TPL	585.60	30.00	4076	38.30	97.58	0.15	0.10	0.50
1344	1	IMXL	616.34	10.00	3876	37.55	89.33	1.99	0.11	0.93
1347	1	TPL	204.51	2.40	2686	37.50	93.94	0.80	0.12	1.04
1350	1	TPL	142.97	9.90	2805	37.14	96.95	0.25	0.12	1.00
1352	1	IMXL	354.71	13.60	4251	37.07	88.43	0.45	0.11	0.70
1353	1	TPL	321.88	2.00	2680	36.96	95.23	1.62	0.11	0.79

1357	1	IMXL	225.85	4.10	4713	36.36	89.39	0.42	0.14	3.98
1359	1	EPL	139.85	8.20	38	36.01	116.20	0.87	0.16	0.44
1364	1	TPL	100.81	11.00	4881	35.93	90.64	0.10	0.20	2.00
1366	1	TPL	220.78	16.70	4870	35.75	90.18	0.30	0.11	0.50
1367	1	TPL	261.40	16.60	4475	35.74	92.89	0.55	0.14	1.04
1369	1	TPL	300.10	12.60	4886	35.58	91.09	0.31	0.12	1.44
1370	1	TPL	255.38	14.70	4753	35.55	91.92	0.41	0.15	1.23
1371	1	TPL	231.17	42.70	4081	35.30	98.57	1.25	0.10	0.66
1372	1	TPL	208.99	6.40	4787	35.30	89.27	0.17	0.15	1.13
1373	1	IMXL	165.96	9.60	4844	35.21	79.86	0.33	0.10	1.00
1374	1	TPL	269.64	5.50	4772	35.22	90.31	0.30	0.10	1.00
1375	1	TPL	198.59	16.00	4688	35.21	92.19	1.75	0.14	0.30
1377	1	TPL	617.76	17.40	4267	34.94	97.69	0.24	0.17	0.99
1378	1	TPL	248.04	35.70	5080	35.03	81.08	0.32	0.12	0.71
1379	1	TPL	121.34	8.00	4960	35.04	83.13	0.20	0.12	1.00
1382	1	TPL	107.02	8.50	4904	34.95	81.56	0.54	0.20	0.80
1383	1	EPL	237.73	1.10	32	35.00	116.84	1.53	0.18	4.73
1385	1	TPL	520.58	9.00	4290	34.91	97.25	0.40	0.10	2.00
1386	1	TPL	372.84	19.30	4855	34.81	90.36	0.25	0.11	0.50
1387	1	TPL	108.03	7.20	4857	34.77	90.65	0.25	0.11	1.00
1388	1	EPL	175.30	3.00	28	34.60	117.26	0.77	0.30	1.00
1389	1	TPL	268.13	22.50	4818	34.57	89.00	1.75	0.14	0.30
1391	1	TPL	127.93	8.00	4920	34.21	82.32	0.25	0.20	1.00
1395	1	TPL	113.96	20.00	4961	34.15	79.78	0.25	0.10	0.60
1396	1	EPL	247.63	3.90	17	34.11	118.21	0.63	0.27	4.03
1399	1	TPL	347.02	45.10	4812	34.01	81.64	0.20	0.10	0.30
1401	1	TPL	105.06	19.70	4525	33.95	80.91	0.80	0.10	1.00
1402	1	TPL	101.50	12.80	5062	33.85	88.59	0.40	0.13	1.42

1403	1	TPL	332.93	50.00	4239	33.60	79.70	1.65	0.11	0.62
1404	1	TPL	472.55	25.70	4935	33.49	90.36	0.51	0.10	0.82
1405	1	TPL	378.99	20.00	4929	33.38	89.87	0.51	0.10	0.82
1411	1	TPL	106.31	5.10	4872	33.01	89.81	1.13	0.14	0.25
1416	1	EPL	703.14	7.90	2	32.81	119.28	1.86	0.49	0.41
1417	2	EPL	286.45	72.90	134	32.68	111.56	0.73	0.14	0.49
1419	1	TPL	149.16	8.20	4615	32.46	89.98	0.50	0.10	1.00
1422	1	TPL	207.16	12.70	4568	32.08	90.87	0.51	0.11	1.43
1424	1	TPL	188.28	33.70	4585	32.03	91.47	1.14	0.10	0.72
1425	1	TPL	251.56	8.50	4465	31.90	87.54	0.25	0.10	1.50
1427	1	TPL	134.17	11.90	4551	31.70	91.17	0.25	0.10	0.80
1428	1	TPL	346.70	19.20	4554	31.71	88.03	0.27	0.18	0.95
1429	1	TPL	267.15	37.90	4563	31.55	88.77	0.25	0.10	0.50
1430	1	EPL	786.91	2.60	5	31.57	117.45	0.63	0.12	4.35
1431	1	TPL	498.06	10.00	4716	31.54	82.98	2.65	0.13	1.00
1433	1	TPL	148.14	12.20	4529	31.51	90.97	0.20	0.13	1.00
1434	1	EPL	161.56	2.90	0	31.58	119.82	0.68	0.15	4.28
1436	1	EPL	206.35	3.70	4	31.47	118.88	0.73	0.30	1.00
1437	1	TPL	146.74	2.30	4424	31.41	84.07	0.70	0.10	2.00
1438	1	EPL	124.24	1.70	1	31.43	120.79	1.34	0.19	4.58
1439	1	TPL	477.00	32.10	4649	31.14	88.36	0.33	0.14	0.73
1440	1	TPL	200.64	18.30	4560	31.25	90.59	0.48	0.10	0.97
1441	1	TPL	144.14	38.30	4666	31.22	91.17	0.51	0.10	0.69
1442	1	TPL	182.53	18.80	4760	31.28	83.47	0.20	0.10	1.00
1443	1	TPL	105.95	11.30	4623	31.24	84.96	0.30	0.10	1.00
1444	1	TPL	101.75	14.60	4629	31.22	89.20	0.50	0.10	1.24
1445	1	TPL	473.71	34.10	4567	31.13	84.12	0.28	0.23	0.72
1446	1	EPL	145.01	4.70	5	31.10	118.99	0.86	0.78	0.56

1447	1	TPL	389.33	8.70	4685	31.02	87.16	0.40	0.10	1.00
1448	1	TPL	102.74	5.30	4656	30.94	89.64	0.80	0.10	1.00
1449	1	TPL	958.10	25.00	4612	30.91	85.61	0.49	0.11	0.83
1450	1	TPL	825.06	120.00	4535	31.06	86.58	1.80	0.12	0.31
1451	1	TPL	141.17	15.10	5101	30.88	83.59	0.20	0.10	1.00
1452	1	TPL	261.27	32.50	4570	30.72	81.22	0.32	0.20	0.73
1454	1	TPL	413.60	44.80	4585	30.68	81.49	0.19	0.13	0.65
1456	1	EPL	128.23	2.90	27	30.45	112.46	1.04	0.14	4.28
1457	1	TPL	205.49	36.30	4714	30.28	86.41	0.17	0.24	0.70
1458	1	EPL	302.36	7.40	16	30.23	114.49	0.63	0.13	3.15
1459	1	TPL	141.90	37.90	5198	30.23	84.79	0.55	0.10	0.69
1460	1	EPL	128.37	5.70	9	30.17	116.45	1.03	0.41	0.45
1461	1	EPL	261.58	6.00	9	30.03	116.35	1.03	0.41	0.45
1462	1	EPL	101.95	5.20	17	30.03	114.21	0.86	0.78	0.56
1463	1	EPL	302.31	5.50	9	29.97	116.22	1.86	0.49	0.41
1464	1	EPL	215.13	2.20	19	29.86	113.30	1.15	0.64	0.26
1465	1	TPL	110.98	18.30	5145	29.85	85.73	0.26	0.10	0.97
1467	*2*	*EPL*	*424.57*	*50.90*	*100*	*29.60*	*118.96*	*1.00*	*0.70*	*0.70*
1470	1	EPL	143.81	3.00	19	29.33	112.97	0.80	0.17	4.25
1472	2	EPL	201.81	39.20	55	29.28	115.21	0.34	0.17	0.69
1473	3	TPL	566.97	28.20	4442	28.98	90.92	0.27	0.11	0.77
1474	1	TPL	277.69	58.30	4580	28.90	85.61	0.31	0.16	0.57
1476	1	EPL	151.81	7.50	14	28.51	116.31	0.38	0.18	0.49
1477	1	TPL	283.19	36.40	5013	28.56	90.40	0.37	0.11	0.70
1479	*1*	*YGPL*	*242.26*	*40.00*	*1962*	*25.78*	*100.18*	*0.57*	*0.18*	*0.68*
1483	*1*	*YGPL*	*298.34*	*19.70*	*1886*	*24.85*	*102.72*	*0.33*	*0.10*	*0.29*
1485	*1*	*YGPL*	*215.37*	*65.30*	*1721*	*24.49*	*102.89*	*0.14*	*0.23*	*0.52*
14153	1	NPML	73.78	1.80	125	45.92	124.45	1.99	0.11	0.93

14177	1	NPML	98.83	2.10	125	45.71	123.87	1.13	0.14	0.25
14316	2	NPML	58.11	25.80	182	43.88	125.83	1.13	0.14	0.25
14520	1	IMXL	86.94	2.70	1218	40.57	112.69	0.77	0.10	1.43
14765	1	TPL	54.33	1.70	2814	37.29	96.90	0.30	0.10	3.00
14800	1	TPL	82.42	1.60	2680	36.91	95.92	0.77	0.10	1.43
14821	1	EPL	99.99	3.90	33	36.42	119.46	0.96	0.12	1.47
14845	1	TPL	80.39	7.80	4856	36.01	88.77	1.62	0.11	0.50
14864	1	TPL	87.44	10.50	4858	35.81	89.43	0.30	0.10	0.70
14872	1	TPL	53.69	8.00	4886	35.70	91.38	0.30	0.10	1.00
14878	1	TPL	99.99	17.40	4911	35.61	90.56	0.43	0.11	0.99
14884	1	TPL	91.01	9.90	5049	35.57	82.76	0.30	0.10	1.00
14894	1	TPL	59.34	6.20	4778	35.43	84.66	0.40	0.10	3.45
14895	1	TPL	64.77	3.20	4815	35.41	88.37	0.25	0.11	2.00
14898	1	TPL	53.86	3.70	4783	35.33	91.87	0.78	0.10	4.08
14901	1	TPL	86.02	7.60	4889	35.30	83.12	0.61	0.12	1.12
14908	1	TPL	51.96	4.30	4772	35.20	90.50	0.77	0.10	1.00
14913	1	TPL	81.87	3.20	4793	35.12	86.73	0.54	0.10	4.20
14940	1	TPL	53.82	3.70	4805	34.81	92.22	0.30	0.12	2.00
14943	1	TPL	71.81	7.50	5039	34.74	81.90	0.30	0.25	0.60
14948	1	IMXL	50.75	4.70	5187	34.69	79.70	0.54	0.10	1.00
14954	1	TPL	97.70	10.60	5004	34.62	80.45	0.15	0.10	1.00
14959	1	TPL	91.22	21.50	5194	34.53	81.05	0.20	0.10	0.60
14966	1	TPL	61.08	9.90	5099	34.48	81.80	0.25	0.10	1.00
14972	1	TPL	61.93	16.10	5100	34.44	81.95	0.25	0.11	0.70
14977	1	TPL	87.28	35.10	5166	34.40	85.78	0.15	0.20	0.30
14984	1	TPL	57.48	9.40	4885	34.34	85.23	0.30	0.12	1.00
15013	1	TPL	80.93	9.80	4922	33.89	91.20	0.25	0.10	1.00
15014	1	TPL	67.52	2.30	4836	33.87	87.02	1.00	0.10	1.50

15026	1	TPL	63.34	5.40	4947	33.63	89.71	0.50	0.10	1.00
15062	1	TPL	57.10	2.50	4822	32.98	88.69	0.40	0.10	3.00
15063	1	TPL	64.98	1.70	4557	32.97	86.72	0.40	0.10	2.00
15064	2	EPL	77.81	21.30	52	33.03	114.26	1.91	0.72	0.27
15135	1	TPL	93.44	5.80	4340	32.11	83.54	0.73	0.10	1.00
15142	1	TPL	93.66	22.90	4467	32.03	84.12	0.77	0.10	0.88
15146	1	TPL	61.22	4.90	4515	32.00	88.23	0.30	0.10	1.50
15160	1	TPL	60.20	7.10	4718	31.86	83.16	1.75	0.14	0.30
15163	1	TPL	88.15	30.70	4553	31.82	88.21	0.37	0.10	0.74
15169	1	TPL	58.80	6.80	4683	31.72	90.74	0.30	0.20	1.00
15175	1	TPL	53.09	8.60	4800	31.62	82.34	1.75	0.14	0.30
15178	1	TPL	54.89	8.80	4605	31.58	87.28	0.20	0.20	1.50
15180	1	TPL	54.07	8.80	4464	31.57	86.75	0.40	0.10	1.00
15184	1	EPL	83.49	2.20	0	31.61	119.55	0.86	0.21	4.45
15191	1	TPL	70.30	4.80	4523	31.47	91.50	0.20	0.20	1.20
15197	1	TPL	72.23	25.80	4648	31.38	87.91	0.69	0.12	0.82
15208	1	TPL	75.95	3.50	4524	31.30	91.46	0.73	0.10	4.13
15232	1	TPL	81.23	10.00	4675	31.07	89.04	1.13	0.14	0.25
15245	1	TPL	58.45	10.80	5116	30.98	82.23	0.30	0.10	1.00
15252	1	TPL	70.76	7.00	4692	30.98	87.41	0.50	0.10	1.50
15257	1	TPL	56.08	4.80	4658	30.93	89.84	0.50	0.10	2.00
15265	1	TPL	65.39	20.10	4657	30.76	84.98	0.50	0.10	0.70
15267	1	TPL	60.05	17.30	4640	30.81	84.79	0.41	0.11	0.99
15270	1	EPL	71.47	2.80	6	30.85	117.11	1.15	0.64	0.26
15276	1	TPL	58.81	6.60	4784	30.63	82.15	0.40	0.10	1.50
15277	1	TPL	84.68	15.50	4684	30.67	86.22	0.31	0.14	1.15
15278	1	TPL	59.30	30.80	4684	30.61	86.31	0.31	0.11	0.74
15292	1	TPL	81.06	10.40	5387	30.43	84.07	0.10	0.13	2.30

15296	1	TPL	68.93	6.70	4807	30.47	88.61	0.35	0.10	1.50
15381	1	EPL	80.79	2.30	22	29.21	112.51	0.86	0.78	0.56
15405	1	TPL	61.67	5.10	4616	28.68	91.68	1.20	0.14	0.30
15424	1	TPL	62.15	4.40	4472	28.14	89.35	1.20	0.30	0.30
15431	*1*	*YGPL*	*50.03*	*51.30*	*2692*	*27.71*	*100.79*	*1.60*	*0.20*	*0.61*
15455	*1*	*YGPL*	*74.75*	*41.70*	*1500*	*26.55*	*100.67*	*0.27*	*0.62*	*0.63*

References (Supplementary Materials)

[1] Hou X, Feng L, Dai Y, et al. Global mapping reveals increase in lacustrine algal blooms over the past decade. Nat Geosci 2022; 15: 130-134.

[2] Shi K, Zhang Y, Zhou Y, et al. Long-term MODIS observations of cyanobacterial dynamics in Lake Taihu: Responses to nutrient enrichment and meteorological factors. Sci Rep 2017; 7: 1-16.